ARTICLE

Covalently linked hopanoid-lipid A improves outer-membrane resistance of a *Bradyrhizobium* symbiont of legumes

Alba Silipo[1,*], Giuseppe Vitiello[1], Djamel Gully[2], Luisa Sturiale[3], Clémence Chaintreuil[2], Joel Fardoux[2], Daniel Gargani[4], Hae-In Lee[5], Gargi Kulkarni[6], Nicolas Busset[2], Roberta Marchetti[1], Angelo Palmigiano[3], Herman Moll[7], Regina Engel[8], Rosa Lanzetta[1], Luigi Paduano[1], Michelangelo Parrilli[1], Woo-Suk Chang[5,9], Otto Holst[8], Dianne K. Newman[6], Domenico Garozzo[3], Gerardino D'Errico[1], Eric Giraud[2,*] & Antonio Molinaro[1,*]

Lipopolysaccharides (LPSs) are major components of the outer membrane of Gram-negative bacteria and are essential for their growth and survival. They act as a structural barrier and play an important role in the interaction with eukaryotic hosts. Here we demonstrate that a photosynthetic *Bradyrhizobium* strain, symbiont of *Aeschynomene* legumes, synthesizes a unique LPS bearing a hopanoid covalently attached to lipid A. Biophysical analyses of reconstituted liposomes indicate that this hopanoid-lipid A structure reinforces the stability and rigidity of the outer membrane. In addition, the bacterium produces other hopanoid molecules not linked to LPS. A hopanoid-deficient strain, lacking a squalene hopene cyclase, displays increased sensitivity to stressful conditions and reduced ability to survive intracellularly in the host plant. This unusual combination of hopanoid and LPS molecules may represent an adaptation to optimize bacterial survival in both free-living and symbiotic states.

[1] Dipartimento di Scienze Chimiche, Complesso Universitario Monte Sant'Angelo, Università di Napoli Federico II, Via Cintia 4, Napoli I-80126, Italy. [2] IRD, Laboratoire des Symbioses Tropicales et Méditerranéennes (LSTM), UMR IRD/SupAgro/INRA/UM2/CIRAD, TA-A82/J, Campus de Baillarguet, 34398 Montpellier cedex 5, France. [3] CNR–Istituto per i Polimeri, Compositi e Biomateriali IPCB, Unità di Catania Via P. Gaifami 18, Catania 95126, Italy. [4] CIRAD, UMR BGPI, Montpellier F-34398, France. [5] Department of Biology, University of Texas, Arlington, Texas, USA. [6] Division of Biology and Biological Engineering, California Institute of Technology and Howards Hughes Medical Institute, Pasadena, California 91125, USA. [7] Division of Bioanalytical Chemistry, Research Center Borstel, Leibniz-Center for Medicine and Biosciences, Parkallee 4a/c, D-23845 Borstel, Germany. [8] Division of Structural Biochemistry, Research Center Borstel, Leibniz-Center for Medicine and Biosciences, Parkallee 4a/c, D-23845 Borstel, Germany. [9] Division of Biotechnology, College of Environmental and Bioresource Sciences, Chonbuk National University, Iksan 570-752, Republic of Korea. * These authors contributed equally to this work. Correspondence and requests for materials should be addressed to A.S. (email: silipo@unina.it) or to E.G. (email: eric.giraud@ird.fr) or to A.M. (email: molinaro@unina.it).

Hopanoids, pentacyclic triterpenoids, constitute an important class of membrane lipids widely distributed in diverse bacteria[1–3]. These molecules, used by geobiologists as 'biomarkers' to assess patterns of bacterial distribution in both ancient and modern ecosystems[4], display structural similarity with eukaryotic sterols[5]. Hopanoids are thought to stabilize membranes, control fluidity and permeability and bolster the integrity of bacterial cell envelope[6].

Lipopolysaccharides (LPSs) are components of the outer membrane of Gram-negative bacteria. Their structural and functional properties are diverse, ranging from restricting the permeability of the outer membrane to playing a central role in bacterial invasion and adaptation to the host environment[7,8]. The general structure of LPS consists of a hydrophilic portion composed of a distal polysaccharide, which in most cases represents the O-antigen, and a proximal oligosaccharide, termed the core, which, in turn, is linked to a glycolipid moiety named lipid A. Noteworthy, in both mammal and plant cells, lipid A is responsible for the interaction with host receptors[7].

Rhizobia are Gram-negative soil bacteria that can establish a symbiotic relationship with legumes, where the bacteria provide the plant with a source of nitrogen[9,10]. Their ability to fix nitrogen from natural sources holds promise as a viable alternative to the use of industrial N-fertilizer in agriculture[11,12]. In rhizobia, LPSs play a role throughout the symbiotic process and their structures are altered in response to plant signals[8,13]. The remarkable structural diversity in the O-antigen region observed among rhizobial species is believed to be a strategy to modulate or suppress plant defence responses, thus facilitating the establishment of symbiosis[14]. Furthermore, the lipid A of rhizobial LPS, characterized by a peculiar lipid and sugar composition and by the presence of very long-chain fatty acids (VLCFA), is important in their adaptation to the intracellular life[14–16].

Photosynthetic bradyrhizobia elicit nitrogen-fixing nodules on roots and stems of some tropical legumes belonging to the *Aeschynomene* genus. Unlike other rhizobia, they lack the canonical *nodABC* genes required for the synthesis of Nod factors (NFs), the signal molecules that initiate symbiosis and which had been thought to be universal to all rhizobium–legume interactions[17]. This finding suggests alternative symbiotic strategies and different molecular patterns involved in NF-independent symbiosis, in which the LPS might play an important role. Previously, we showed that the Nod-independent *Bradyrhizobium* BTAi1 strain suppresses basal defence in plants through an LPS composed of a unique monosaccharide[18].

In the present study, we demonstrate that BTAi1 also builds a unique LPS lipid A that is covalently substituted by a hopanoid structure. In addition, BTAi1 produces other hopanoids that are not linked to LPS. By constructing a hopanoid-deficient mutant, we show that hopanoids are essential for both free-living and symbiotic life of the bacteria.

Results

Structure of the lipid A from *Bradyrhizobium* BTAi1. The primary structure and the supramolecular arrangement of the lipid A isolated from BTAi1 were obtained using mass spectrometry (MS), nuclear magnetic resonance (NMR) spectroscopy, electron spin resonance (ESR) spectroscopy and dynamic light scattering (DLS). These different analytical methods revealed the presence of a novel hopanoid molecule as an LPS constituent. Representative depictions of this unique lipid A structure (compound **1**) are illustrated in Figs 1 and 2; further details on the in-depth characterization are presented in Supplementary Notes 1–4 and Supplementary Tables 1–3.

Briefly, the positive ion matrix-assisted laser desorption ionization (MALDI) spectrum of lipid A (Fig. 1b) exhibited a heterogeneous mixture of ion peaks, present as Na^+ adducts, belonging to three families of molecules differing in their acylation pattern, namely, in the lipid chain nature and content; for each family, the mass differences between neighbouring ions were due to the different lengths and/or substitution patterns of the ester-linked acyl chains (Supplementary Note 3, Supplementary Figs 1–3). The lowest molecular mass peak at m/z 2,128.42 was identified as a penta-acylated form possessing two 14:0(3-OH), one 12:0(3-OH) one 12:1 and one acetylated VLCFA, 26:0 (25-OAc); no additional peaks were observed in this mass range. The mass peak at m/z 2,622.96 carried an additional secondary VLCFA recognized as 32:0(2,31-2OH). The third lipid A ion cluster showed an analogous acylation pattern shifted at higher molecular mass by $\Delta m/z$ 512.4. The mass difference (fit with a molecular formula $C_{34}H_{56}O_3$) matched the hopanoid residue identified using GC-MS and NMR analyses. MS/MS analysis of the ion species at m/z 3,135.36 (Figs 1c and 2, Supplementary Note 3) indicated that the hopanoid moiety was a tertiary substituent, located at the ω-1 position of the long-chain fatty acid as deduced using NMR. This latter approach (see Supplementary Note 4, Supplementary Table 2 and Supplementary Figs 4–7) allowed us to establish the full structure of lipid A from BTAi1 (Fig. 2). It consisted of an invariable pentasaccharide sugar backbone formed by a skeleton of β-(1→6)-linked 2,3-diamino-2,3-dideoxy-D-glucopyranose (DAG) carrying an α-GalpA on the vicinal DAG and an α-(1→6) Manp disaccharide on the distal DAG unit, substituted by a heterogeneous blend, in terms of number and nature, of lipid chains asymmetrically distributed on the sugar skeleton. The two secondary VLCFAs were substituted by a hopandiolic acid and by an acetyl group. Interestingly, of the two VLCFAs, the O-acetylated one did not vary among all the lipid A species, while the other bearing the hopanoid residue was responsible for the observed heterogeneity in terms of length and hydroxylation pattern (Figs 1b and 2). Although the occurrence of *Bradyrhizobium* species containing lipid A with two, three or even four VLCFAs has been already reported[19], the presence of a hopanoid molecule covalently attached to lipid A had never been described in any LPS including those from non-photosynthetic *Bradyrhizobium* strains[19–22]. This represents a novel lipid A skeleton, which we name HoLA for Hopanoid-Lipid A.

Analysis of hopanoid lipids present in *Bradyrhizobium* BTAi1. As most hopanoid-producing bacteria make a suite of hopanoids found within their inner and/or outer membranes[23–26], we investigated the triterpenoid content of BTAi1 using GC-MS. Our data showed that it synthesized several hopanoids, including desmethyl and 2-methyl versions of diploptene, diplopterol and bacteriohopanetetrol (Fig. 3). We were also able to detect BHP-550, which was most likely a degradation product of bacteriohopaneaminotriol. BTAi1 also produced tetrahymanol, a triterpenoid with a gammacerane skeleton. This indicated that BTAi1 possessed both 'free' and lipid A-bound hopanoids.

Construction of a hopanoid-deficient mutant. To investigate the biological significance of free as well as lipid A-bound hopanoids, we constructed a hopanoid *minus* mutant. A key step in the biosynthesis of hopanoids is the cyclization of the linear squalene into the pentacyclic triterpenoid hopene catalysed by squalene hopene cyclase (Shc)[27]. Genome sequence analysis of photosynthetic *Bradyrhizobium* strains revealed the presence of only one *shc* gene, which, in contrast to the non-photosynthetic strains, was not surrounded by other genes involved in hopanoid biosynthesis (Supplementary Fig. 8a). The hopanoid-deficient
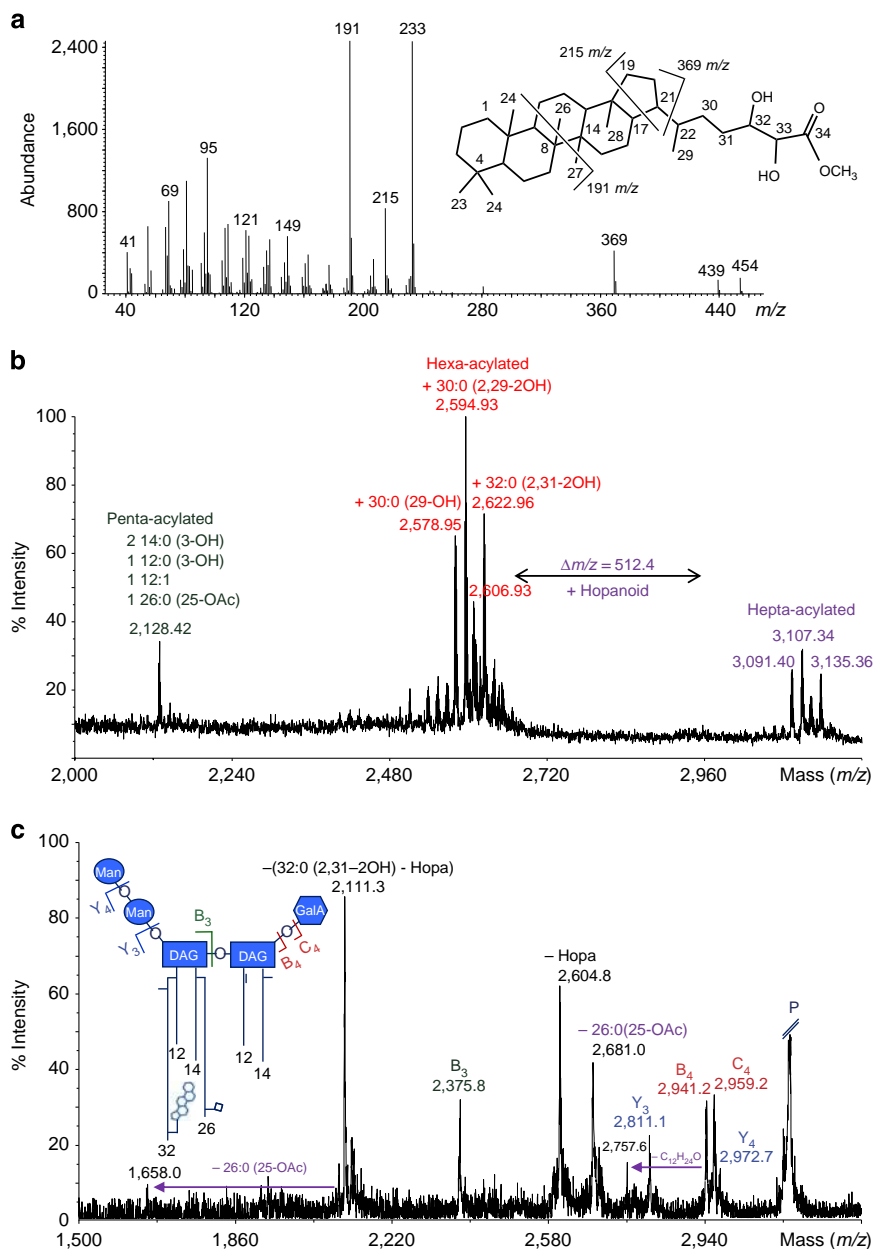
Figure 1 | MS analysis of *Bradyrhizobium* BTAi1 lipid A. (**a**) Mass spectrum of carboxy-methylated hopanoid derivative as obtained by GC-MS analysis of the lipid A; the hopanoid numbering and fragmentation pattern are reported in the inset. (**b**) Reflectron MALDI TOF mass spectrum in positive ion more of the lipid A from *Bradyrhizobium* BTAi1; ion peaks are present as Na$^+$ adducts. (**c**) MALDI TOF/TOF MS^2 analysis of the hepta-acylated lipid A species at *m/z* 3135.36 (P: parent ion). The lipid A is sketched, letters refer to the ions generated in the MS/MS spectrum. The square indicates the acetyl group, the hopanoid is schematically indicated with the pentacyclic triterpenoid moiety (DAG, 2,3-diamino-2,3-dideoxy-D-glucopyranose; GalA, galacturonic acid; Man, mannose; Hopa, hopanoid).

mutant (BTAi1Δ*shc*) was constructed by deleting *shc*, and GC/ MS analysis of the total lipid extract (TLE) confirmed that this mutant did not produce any type of hopanoid, including that linked to lipid A (Fig. 3). In parallel, we isolated and purified LPS from *Bradyrhizobium* BTAi1Δ*shc* to check whether the mutation had any effect on lipid A structure. Our chemical, NMR and MS analyses showed that BTAi1Δ*shc* LPS was identical to BTAi1WT LPS, with the exception of the absence of the hopanoid substitution in the mutant (Supplementary Fig. 9). This finding suggested that lipid A biosynthesis preceded its attachment to a hopanoid moiety. The enzyme(s) that catalyse(s) the covalent attachment of hopanoids to lipid A remain(s) to be discovered.

Role of hopanoids in bacterial physiology. As the absence of hopanoids in the membranes could modify their stability and therefore have a profound impact on BTAi1 physiology, we analysed the effect of the *shc* mutation on the growth of BTAi1 in both rich and minimal media. As shown in Fig. 4a,b, the growth rate of the mutant was markedly lower than that of the WT strain in both media. When we lowered the growth temperature to 30 or 25 °C to increase membrane stability, we still observed that the mutant grew less well than the WT; however, the difference in growth rates was less pronounced (Supplementary Fig. 10). Notably, deletion of the *shc* gene in other bacteria, such as *Rhodopseudomonas palustris* TIE-1, a phylogenetically related species to photosynthetic bradyrhizobia,
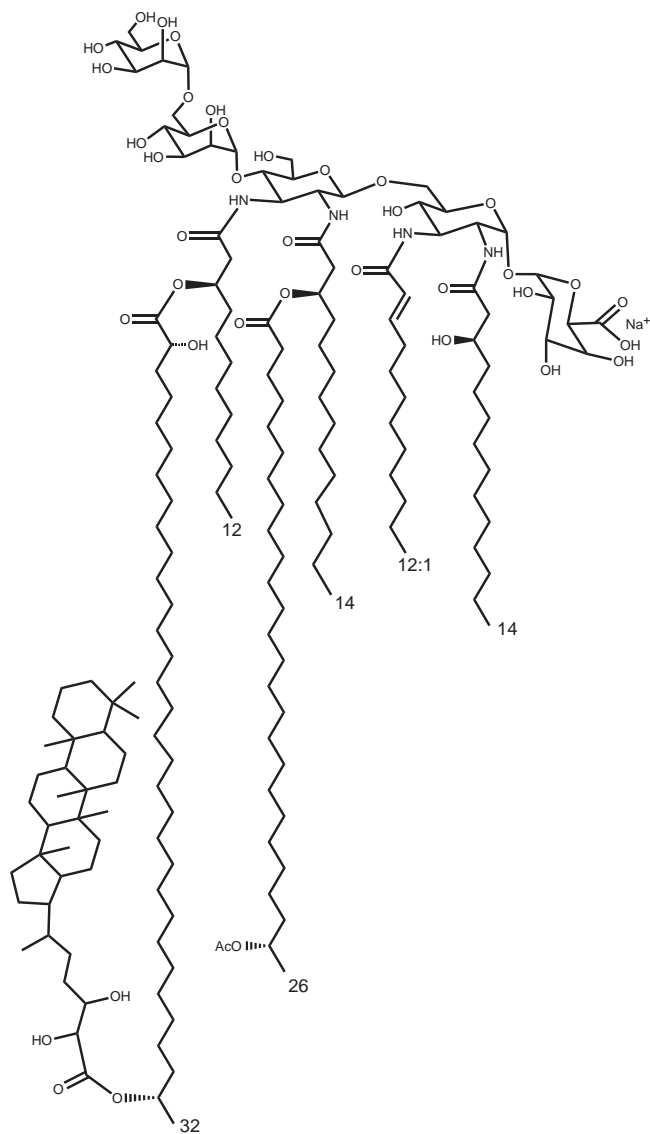
3

Figure 2 | *Bradyrhizobium* BTAi1 lipid A structure. *Bradyrhizobium* BTAi1 lipid A structure of the hepta-acylated ion species at *m/z* 3,135.36 (compound **1**).

does not alter its growth rate at 30 °C under normal culture conditions[28].

Hopanoids are thought to act as membrane condensers, thus increasing bacterial resistance to various abiotic stresses[6,29–31]. This prompted us to evaluate the ability of BTAi1Δ*shc* mutant to cope with various stressors. We tested oxidative, acid and detergent stresses using disk diffusion assays. Saline/osmotic stress was evaluated by comparing bacterial growth rates in the presence of increasing concentrations of NaCl. The data obtained (Fig. 4c,d) showed that the BTAi1Δ*shc* mutant was more sensitive than the WT strain to all stressors tested. Reintroduction of the *shc* gene under a constitutive promoter (P*nptII*) into the Δ*shc* mutant restored growth and higher stress resistance under all conditions (Fig. 4), excluding the possibility of polar effects or secondary mutation. These data indicated that hopanoids play an important role in the physiology of BTAi1.

Role of hopanoids in symbiosis. To determine whether hopanoids facilitate symbiosis, we infected the legume *Aeschynomene evenia* with both WT and Δ*shc* mutant BTAi1 strains and
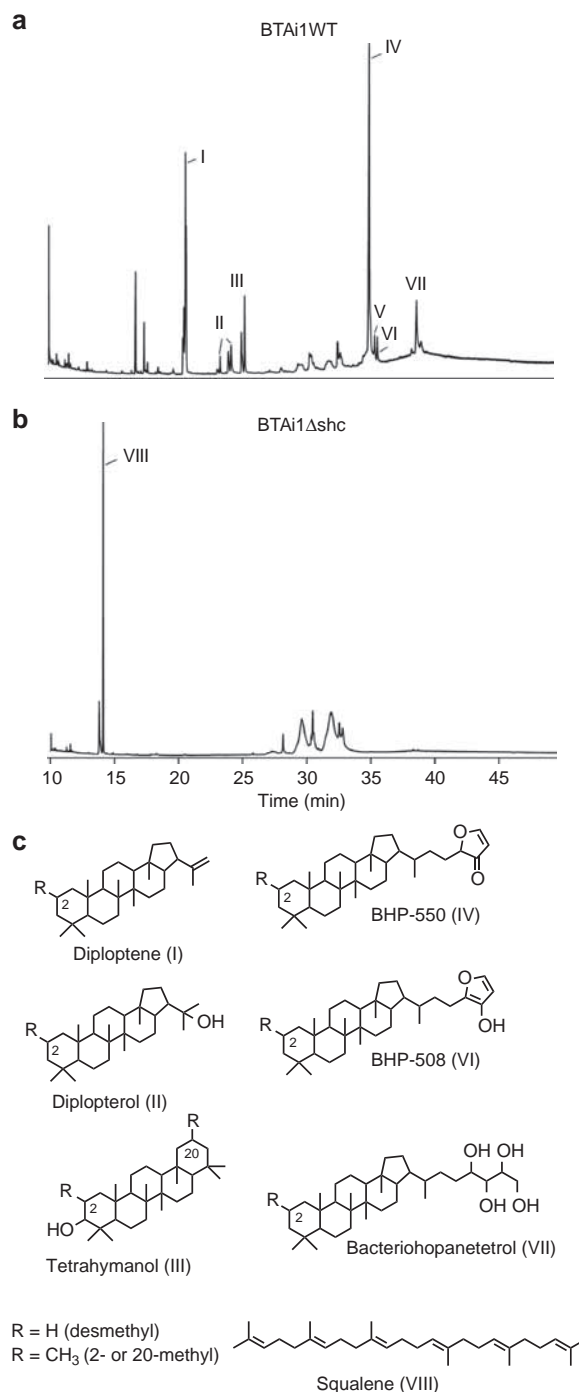

Figure 3 | GC-MS total ion chromatograms of acetylated total lipid extracts from BTAi1 strains. (**a**) *Bradyrhizobium* strain BTAi1 and (**b**) *Bradyrhizobium* strain BTAi1Δ*shc*. Main hopanoid peaks are numbered and the 2-methyl counterparts elute 0.2–0.5 min earlier: I, diploptene (desmethyl and 2-methyl); II, diplopterol (desmethyl and 2-methyl); III, tetrahymanol (demethyl, 2-methyl and 20-methyl); IV, BHP-550; V, unidentified BHP; VI, BHP-508; VII, bacteriohopanetetrol (desmethyl and 2-methyl); VIII, squalene. Compounds were identified by comparison of retention times and mass spectra to those of *R. palustris* TIE-1 (ref. 51). Lipid analysis for each strain was performed in triplicates. (**c**) Chemical structures of the isolated hopanoids.

followed the kinetics of nodule formation. The complemented mutant was not tested during this experiment because the pMG103 plasmid used to reintroduce the *shc* gene was not stable
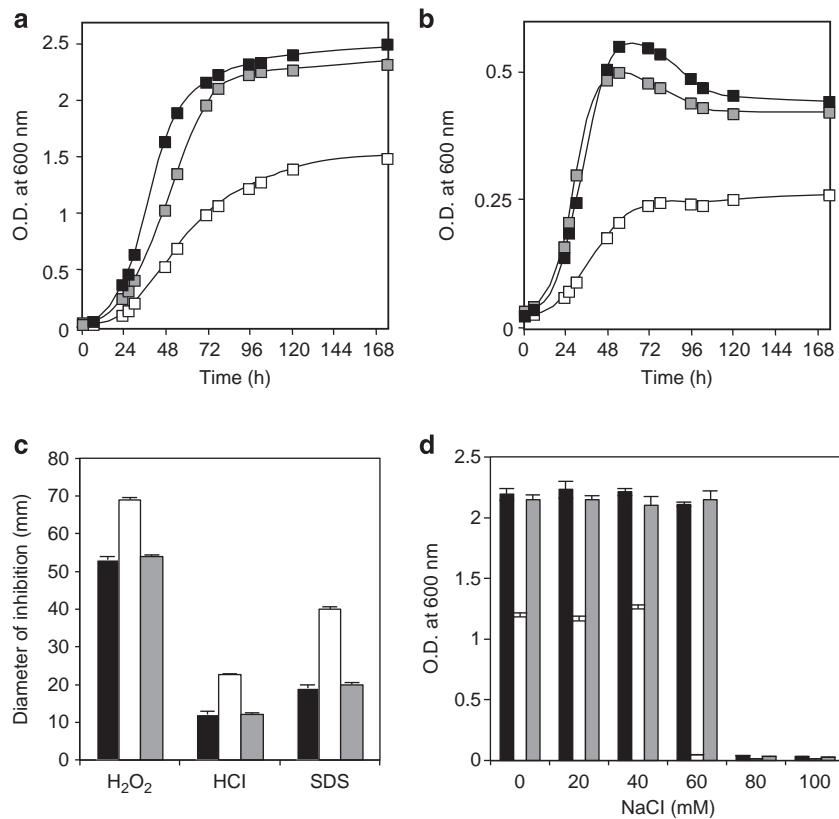
Figure 4 | Physiology of the hopanoid biosynthesis mutant (BTAi1Δ*shc*). (**a**,**b**) Representative growth curves of BTAi1 (black square), BTAi1Δ*shc* (white square) and complemented BTAi1Δ*shc* + *shc* (grey square) strains cultivated in rich (**a**) or minimal medium (**b**). (**c**) Hydrogen peroxide (H_2O_2), hydrogen chloride (HCl) and sodium dodecyl sulfate (SDS) resistance of BTAi1 (black bar), BTAi1Δ*shc* (white bar) and complemented BTAi1Δ*shc* + *shc* (grey bar) strains, as determined by disk diffusion assays using 5 μl of 5.5 M H_2O_2, 2 N HCl or 10% of SDS according to a previously published protocol[63]. Error bars represent s.e. (*n* = 9). (**d**) NaCl resistance of BTAi1 (black bar), BTAi1Δ*shc* (white bar) and complemented BTAi1Δ*shc* + *shc* (grey bar) strains. Error bars represent s.e. (*n* = 3).

in the BTAi1 strain in the absence of selective pressure and the spectinomycin antibiotic could not be used during plant culture. First observations were made after the symbiotic relationship had been well established with the formation of functional nodules[32]. At 6 days post inoculation (d.p.i.), no significant differences were observed between plants inoculated with WT and mutant strains, the number of nodules per plants and the nitrogenase activity measured by the acetylene reduction assay (ARA) were comparable (Fig. 5a,b). This indicated that the Δ*shc* mutation had no effect on the ability of the bacteria to establish a symbiotic relationship. However, at 8 d.p.i., we observed that the plants inoculated with the Δ*shc* mutant fixed nitrogen slightly less efficiently than those inoculated with the WT strain, although the number of nodules elicited by the mutant was significantly higher (Fig. 5a,b). Cytological analysis of nodules (8 d.p.i.) using transmission electronic microscopy (TEM) revealed signs of nodule degeneracy. Although the endosymbiotic BTAi1Δ*shc* strain displayed, as did the WT, a typical spherical shape, indicating that the process of differentiation into bacteroids properly occurred, their size was smaller and the peribacteroid space was larger (Fig. 5c–f). Furthermore, some BTAi1Δ*shc* bacteroids displayed a profoundly perturbed envelope with a clear separation between the inner and outer membranes (Fig. 5f). Some bacteroids were far more drastically affected, with broken cell walls and an electron-dense cytoplasm suggesting that they were dead (Fig. 5g). At latter times (12 and 19 d.p.i.), ARA activity of the plants inoculated with the mutant was only half that of plants inoculated with the WT strain, whereas twice more

nodules per plant were formed with the mutant (Fig. 5a,b). This increase in the nodule number, similar to what had been observed upon infection with a nitrogenase *minus* mutant[33], could be attributed to a phenomenon termed autoregulation of nodulation that ensures a balance between nodule formation and energy requirements in legumes[34]. At these times, we observed typical nitrogen starvation symptoms in the entire plant, for example, foliage chlorosis and reduced plant growth (Fig. 5h). These observations indicated that at early stages of the symbiotic interaction, the mutant was able to engage normally in an efficient association but that its nodules rapidly lost their ability to fix nitrogen. In agreement with this, at 19 d.p.i., the majority of the nodules elicited by the mutant were yellowish instead of green as observed for the WT nodules (Fig. 5i,j), hollow from inside (Fig. 5k), and did not display the red colour typical of leghaemoglobin as observed for the WT nodules (Fig. 5l). TEM observations showed no change in the ultrastructure of the WT nodules (Fig. 5m) in contrast to the mutant nodules for which the symbiotic tissues were digested (Fig. 5n,o). Such symptoms (leghaemoglobin degradation and symbiotic tissue digestion) characterize senescent nodules that occur naturally for WT nodules older than 50 days.

Together, these data showed that hopanoids play a critical role in chronic infection of the plant partner by BTAi1.

Role of HoLA and free hopanoids in outer membrane stability. To test the hypothesis that phenotypic defects observed both *in*
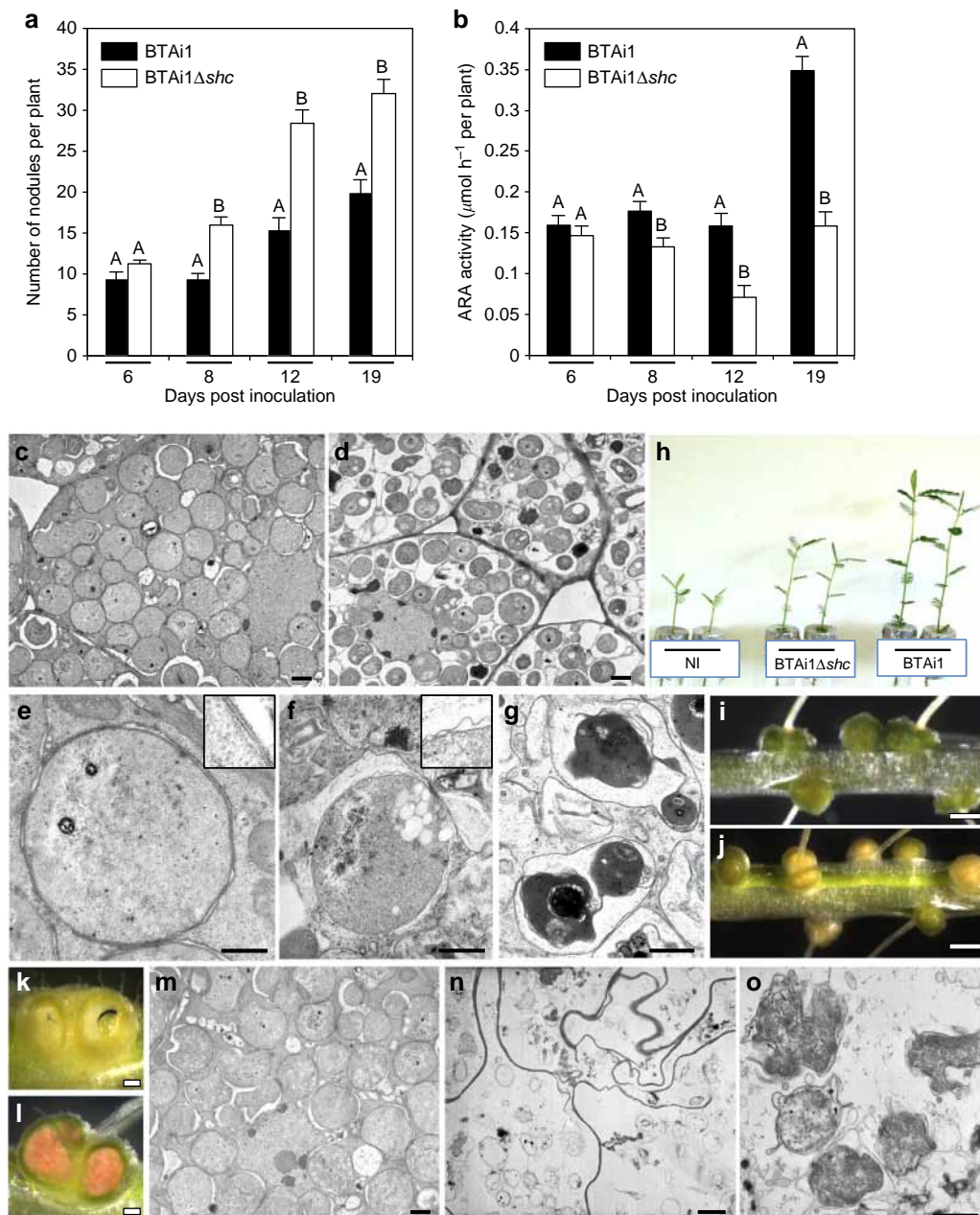
Figure 5 | The BTAi1Δshc mutant is severely impaired in symbiosis with A. evenia. (**a**) Nodulation kinetics of *Bradyrhizobium* BTAi1 and BTAi1Δshc strains on *A. evenia* plants. (**b**) The occurrence of acetylene-reducing activity (ARA) in *A. evenia* plants inoculated with *Bradyrhizobium* BTAi1 and BTAi1Δshc mutant. Error bars in **a,b** represent s.e. ($n = 5$). Different letters above the error bars indicate significant differences at $P < 0.05$ (Tukey's HSD test). (**c–g**) Transmission electron micrographs of nodules elicited by the WT strain (**c,e**) and the BTAi1Δshc mutant (**d,f,g**) at 8 d.p.i. Insets in **e,f** show a detail of the cell wall ultrastructure of bacteroids. Scale bars are 1 μm (**c,d**), and 0.5 μm (**e–g**). (**h**) Comparison of the growth of the plants (aerial part) non-inoculated (NI) or inoculated with BTAi1 or BTAi1Δshc strains (at 19 d.p.i.). (**i–l**) Aspect of the nodules elicited by the WT strain BTAi1 (**i,l**) and the BTAi1Δshc mutant (**j,k**) at 19 d.p.i. Scale bars are 1 mm (**i,j**) and 100 μm (**k,l**). (**m–o**) Transmission electron micrographs of nodules elicited by the WT strain (**m**) and the BTAi1Δshc mutant (**n,o**) at 19 d.p.i. Scale bars are 1 μm (**m,n**) and 0.5 μm (**o**).

planta and *ex planta* for the BTAi1Δshc mutant resulted from the loss of integrity of the external membrane because of the lack of hopanoids, we analysed the ultrastructure of the WT strain and the BTAi1Δshc mutant cultivated in free-living state using TEM. As shown in Fig. 6, the WT cells were rod-shaped, with perfectly defined membranes, whereas the mutant cells displayed morphological distortion and an irregular outer boundary. These observations are consistent with outer membrane deformities previously reported for the Δshc mutant of *R. palustris* TIE-1 (ref. 6).

Furthermore, we investigated the microstructure of membranes from BTAi1 and the Δshc mutant using ESR. We adopted a novel protocol for asymmetric liposome preparation based on the assembly of two independently prepared lipid monolayers (see Methods, Fig. 7a and Supplementary Note 5)[35]. In all cases, a unique distribution of liposome, whose dimension was centred at ~100 nm, was detected (Supplementary Fig. 11). A phosphocholine spin-label on the 5 position of the acyl chain, 1-palmitoyl-2-[5-(4,4 dimethyloxazolidine-*N*-oxyl)]stearoyl-*sn*-glycero-3-phosphocholine (5-PCSL), was included alternatively
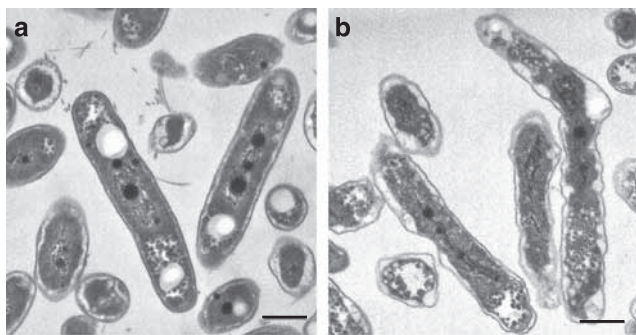
Figure 6 | The BTAi1Δ*shc* cells display membrane defects.
(**a**,**b**) Transmission electron microscopy of BTAi1 (**a**) and BTAi1Δ*shc*
(**b**) cells grown on YM medium and harvested 120 h after inoculation. Scale
bar, 0.5 μm.

in the outer or in the inner lipid leaflet constituting the bilayer, thus allowing a direct detection of the lipid ordering and dynamics.

The ESR spectra showed evident perturbation in asymmetric bilayers including HoLA in the outer leaflet formulation (Fig. 7b, Supplementary Table 4), indicating that HoLA insertion causes lower fluidity of the whole membrane, evocative of mechanical strengthening. In this respect, hopanoids serve the same function as sterols (for example, cholesterol) in eukaryotes[5,36], although they appear to cause a weaker condensing and ordering effect[37]. Unexpectedly, the inner leaflet was even more affected by HoLA presence than the outer leaflet, in which lipid A had been positioned. This indicated that the long acyl chains of HoLA span both layers of the lipid membrane, so that the terminal hopanoid appendages were positioned in the inner leaflet (Fig. 7b). The result of this arrangement was twofold: (i) both leaflets were much more ordered and (ii) the leaflets were tightly linked, the long acyl chains acting as a 'tightrope' between the two membrane surfaces. We also studied asymmetric lipid bilayers including lipid A from the BTAi1Δ*shc* mutant in the outer leaflet formulation. In this case, the ESR spectra showed that the outer leaflet was less fluid than the inner one. Furthermore, the whole bilayer was less ordered than the one containing HoLA. This result indicated that linking the hopanoid moiety to the terminus of one acyl chain drove its insertion into the chains of the opposite leaflet.

Finally, we considered a membrane whose outer leaflet contained the lipid A from the BTAI1Δ*shc* mutant and the hopanoid extract from *Bradyrhizobium* free of HoLA. The ESR spectra showed that only the outer leaflet was affected by the hopanoid-ordering effect, while the inner one remains almost unperturbed; this suggests that, in the absence of the covalent link to the long acyl chain, the hopanoid moiety tends to reside among the lipid A chains of the outer layer.

These findings were supported by ESR results obtained using another spin-labelled lipid, 14-PCSL, bearing the radical reporter group on the 14 position of the acyl chain, thus monitoring the inner part of the bilayer hydrophobic core (see Supplementary Note 5 and Supplementary Fig. 12). It was found that HoLA was able to increase the acyl chain order in the whole membrane profile, including the central section.

In conclusion, our results suggest that the molecular structure of HoLA is well suited to induce ordering of the asymmetric outer membrane, resulting in enhanced mechanical strength and stabilization.

Discussion

Hopanoids were described as abundant constituents of the membranes of *Bradyrhizobium* strains more than two decades
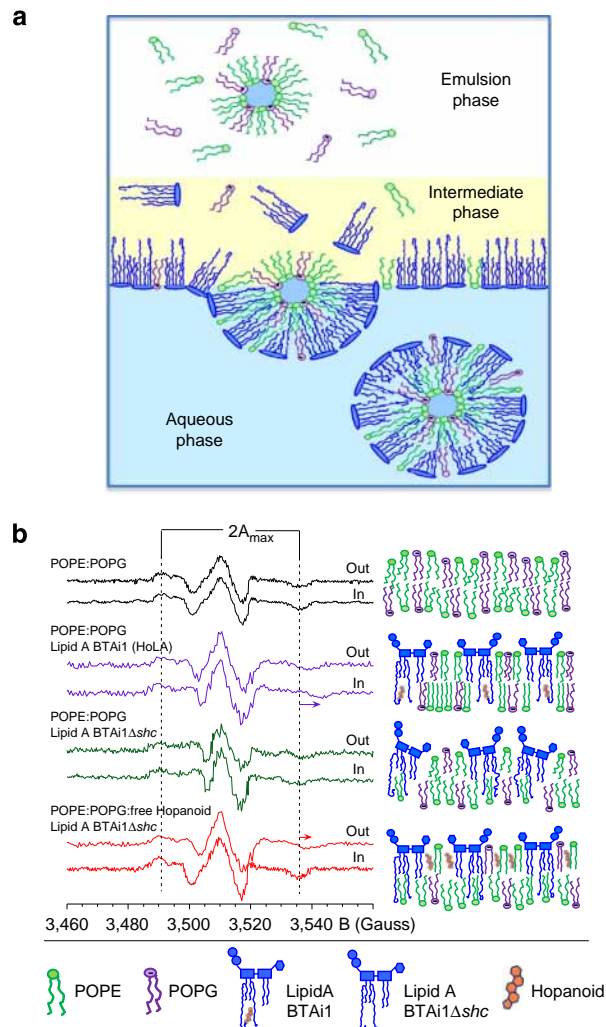

Figure 7 | Physicochemical characterization of *Bradyrhizobium* BTAi1-reconstituted model membrane. (**a**) Schematic representation of asymmetric liposome formulation procedure. (**b**) ESR spectra of 5-PCSL in the outer (out) or inner (in) leaflet of the asymmetric liposomes whose components of the outer leaflet are specified in the figure. The inner leaflet is composed of a POPE/POPG mixture. A quantitative estimation of leaflet order and rigidity is obtained by determining the outer hyperfine coupling constant, $2A_{max}$, as indicated in the figure. Increased $2A_{max}$, as highlighted by the arrows, indicate higher order and/or rigidity. Sketches give a visual qualitative representation of the membranes.

ago. For instance, in *B. diazoefficiens* USDA110, they account for more than 40% of the total lipid fraction[3]. Despite the ecological and agricultural interest of these bacterial strains, we know relatively little about the structural and functional role of hopanoids. Besides the expected presence of 'free' hopanoids in the cell envelope of photosynthetic bradyrhizobia, here we discovered a novel LPS chemical architecture characterized by the covalent attachment of a hopanoid to the lipid A. Such LPS chemical architecture (HoLA) has not been described previously. Although we cannot ascertain the specific roles of HoLA compared with free hopanoids, our physical–chemical analyses, conducted on reconstituted asymmetric bilayers, clearly indicated that the HoLA molecules, spanning the whole outer membrane with the hopanoid located in the inner leaflet, permits a higher ordering and strengthening of both the inner and outer leaflets of the outer membrane, possibly imparting a functional advantage to the bacterium under some conditions. In detail,

Bradyrhizobium BTAi1 synthesized a mixture of lipid A species differing by the number, length and nature of the acyl substitutions, linked or not to hopanoids. The availability of different types of lipid A could be an efficient strategy for BTAi1 to dynamically modulate the fluidity and rigidity of its outer membrane in response to environmental changes.

Several interesting phenotypes arose from the absence of hopanoids in photosynthetic bradyrhizobia. These included growth defects in the presence of different stressors, and an inability to maintain a chronic intracellular infection in a symbiotic context. In the intracellular milieu of the legume cell, the rhizobium has to cope with various stresses such as peribacteroid space acidification[38] and oxidative stress because of the production of reactive oxygen and nitrogen species (H_2O_2, O_2^- and NO) by the host cell[39]. In addition, recent data suggested that *Aeschynomene* use antimicrobial peptides similar to NCR peptides described in *Medicago* to control bacteroid differentiation[40]. It is known that *shc* mutants of some bacterial species are more sensitive to these compounds[41,42]. It could be therefore possible that the symbiotic deficiency of the *shc* mutant resulted from its inability to survive in such a harsh intracellular environment.

Identifying the enzyme(s) that catalyse(s) the attachment of hopanoid to lipid A will enable the precise role of HoLA to be determined as well as allow us to assess the phylogenetic distribution of HoLA among Gram-negative bacteria, assuming that this enzyme is well conserved. In *R. palustris*, a bacterium closely related to *Bradyrhizobium*, all the genes involved in hopanoid biosynthesis are located close together in a DNA region called the hopanoid biosynthetic gene cluster[28]. This cluster is well conserved in all *Bradyrhizobium* strains; however, in photosynthetic bradyrhizobia, the *shc* gene was found elsewhere in the genome. Besides the fact that the gene organization surrounding *shc* is different, phylogenetic analysis showed that *shc* genes from photosynthetic and non-photosynthetic *Bradyrhizobium* form two distant clusters (Supplementary Fig. 8b). A high level of identity was observed between the Shc proteins belonging to the same clade (> at 85%), whereas this identity dropped to only 35% between Shc proteins belonging to different clades. Altogether, these data suggested that the two classes of Shc could have different biochemical properties and functional roles, which could be related to the ability to synthesize HoLA. Experiments are in progress to exchange the *shc* genes between photosynthetic and non-photosynthetic bradyrhizobia to clarify the specific roles of these two Shc types by analysing the impact of this allelic exchange on LPS structure and hopanoid content.

In summary, the discovery that HoLA and hopanoids contribute to the outer membrane structure of photosynthetic bradyrhizobia could have important biotechnology applications. For instance, manipulation of hopanoid biosynthesis could be used either to strengthen this barrier, thus increasing the ability of bacteria to survive stress conditions, or to relax this barrier, thus promoting the exchange of diffusible molecules between the bacteria and the external environment. Future studies will shed light on the specific mechanisms, whereby hopanoids and HoLA enhance cell membrane properties in the context of plant–microbe symbioses.

Methods

Bacterial strains and growth conditions. *Bradyrhizobium* strain BTAi1 and derivatives (BTAi1Δ*shc* and BTAi1Δ*shc* + *shc*) were grown in rich YM medium[43] or BNM (buffered nodulation medium) minimal medium[44] at 37 °C. When required, the media were supplemented with kanamycin (50 µg ml^{-1}) for BTAi1Δ*shc* and a mixture of kanamycin (50 µg ml^{-1}) and spectinomycin (50 µg ml^{-1}) for BTAi1Δ*shc* + *shc*.

Recovery of LPS from *Bradyrhizobium* BTAi1 and BTAi1Δ*shc*. In order to recover the LPS material, bacterial cells were extracted applying the phenol/water method[45] and, after extensive dialyses, the extracted phases were subjected to a step of enzymatic digestions with DNAse, RNAse and protease in order to remove nucleic acid and protein contaminants and recovered using ultracentrifugation (100,000 *g*, 4 °C, 24 h).

Both water and phenol fractions were analysed through SDS–polyacrylamide gel electrophoresis (SDS–PAGE) 13.5%; the LPS fraction was exclusively found in the water phase as suggested by the presence of the typical ladder in its migration pattern in the gel (Supplementary Fig. 13). The LPS fraction was further purified using size filtration chromatography (SephacrylS-400 HR in 50 mM $(NH_4)_2CO_3$ from GE Healthcare; yield 3% of dried material).

Compositional analysis. Sugar content was determined with the GC-MS analysis of acetylated *O*-methyl derivatives. The dried LPS sample was left over a drying agent, under continuous vacuum, for a couple of hours. Then 1 ml of methanolic HCl was added and incubated at 85 °C for 16 h, the sample was dried in a stream of air, subsequently acetylated extract with pyridine (25 µl) and Ac_2O (25 µl), 80 °C, 30 min and analysed using gas-liquid chromatography (GLC)-MS[46]. Linkage analysis was carried out by methylation of the complete core region as described. The sample was hydrolysed with 4 M trifluoroacetic acid (100 °C, 4 h), carbonyl-reduced with $NaBD_4$, carboxy-methylated, carboxyl-reduced, acetylated and analysed using GLC-MS[47].

Total fatty acid content was obtained by acid hydrolysis. LPS was first treated with 4 M HCl (4 h, 100 °C) and then with 5 M NaOH (30 min, 100 °C). Fatty acids were then extracted in $CHCl_3$, methylated with diazomethane and analysed using GLC-MS. The ester-bound fatty acids were selectively released by base-catalysed hydrolysis with 0.5 M NaOH/MeOH (1:1 v/v, 85 °C, 2 h), and then the product was acidified, extracted in $CHCl_3$, methylated with diazomethane and analysed using GLC-MS[48].

Recovery of lipid A from *Bradyrhizobium* BTAi1 and BTAi1Δ*shc*. In order to obtain lipid A, LPS was dissolved in acetate buffer (pH 4.4) and the hydrolysis was run for 5 h at 100 °C. It was purified according to the procedure provided in ref. 49. In brief, adequate amounts of chloroform and methanol were added to the hydrolysate to obtain chloroform/methanol/hydrolysate 2:2:1.8 (v/v/v), and the mixture was vigorously shaken, and then centrifuged. The chloroform phase, containing the lipid A, was collected and washed twice with the water phase from a freshly prepared two-phase Bligh/Dyer mixture (chloroform/methanol/water, 2:2:1.8 (v/v/v))[50]. The organic phases were collected and dried.

Recovery of hopanoid extracts. In order to recover hopanoid lipids, bacterial cells from *Bradyrhizobium* were extracted as follows[3,50]. WT and Δ*shc* cultures were grown in triplicates in 2-l flasks with 200 ml YM medium at 37 °C in dark for *ca.* 72 h. Cultures were harvested using centrifugation at 5,000 *g* for 15 min at 4 °C and the cell pellets frozen at − 80 °C until ready for use. Lipid extraction was performed by resuspending cells in 6 ml of water, 2 ml of which were transferred into Teflon centrifuge tubes (VWR, Bridgeport, NJ). This was followed by addition of 5 ml of methanol (MeOH) and 2.5 ml of dichloromethane (DCM) and sonication for 15 min at room temperature. Samples were centrifuged at 7,000 *g* for 10 min at 22 °C and the supernatants were transferred to new tubes. The cell pellets were resuspended again in 9.5 ml of 10:5:4 MeOH:DCM:H_2O, sonicated and centrifuged and the supernatants were combined with the first extraction. The samples were separated into two phases by adding ~13 ml of DCM and centrifuging at 6,000 *g* for 10 min at 22 °C. The lower organic phase was transferred to a new glass vial and evaporated in a chemical hood overnight (TLE).

The TLE was resuspended in DCM at a concentration of 1 mg ml^{-1}. Hundred microlitres of this extract was evaporated under 60 °C and then derivatized to acetate esters by incubation in 100 µl of 1:1 acetic anhydride:pyridine for 30 min at 60 °C. The acetylated TLEs were analysed using high-temperature GC-MS[51]. Compounds were identified by comparison of retention times and mass spectra with those of *R. palustris* TIE-1 (ref. 6).

NMR spectroscopy. NMR spectra of the lipid A fraction were recorded in $CDCl_3$/MeOD 1:1 at 25 °C, on Bruker 600 DRX equipped with a cryo probe. ROESY (rotating-frame Overhauser effect spectroscopy) and NOESY (nuclear Overhauser effect spectroscopy) experiments were recorded using data sets of (t1 × t2) of 4,096 × 256 points with mixing times at 100–200 ms. Double quantum-filtered phase-sensitive COSY (double quantum-filtered Correlation SpectroscopY) experiments were performed using data sets of 4,096 × 512 points. TOCSY (Total Correlation Spectroscopy) experiments were performed with spinlock times of 100 ms, using data sets (t1 × t2) of 4,096 × 256 points. In all homonuclear experiments, the data matrix was zero-filled in both dimensions to give a matrix of 4 K × 2 K points and was resolution-enhanced in both dimensions by a cosine-bell function before Fourier transformation. Coupling constants were determined by two-dimensional (2D) phase-sensitive DQF-COSY[52,53]. HSQC (Heteronuclear Single Quantum Correlation), *J*-coupled HSQC, HSQC-TOCSY and HMBC (Heteronuclear Multiple-Bond Correlation) experiments were measured in the ^{1}H-detected mode via single quantum coherence with proton decoupling in the ^{13}C

domain, using data sets of 2,048 × 256 points. Experiments were carried out in the phase-sensitive mode[54]. A 60-ms delay was used for the evolution of long-range connectivities in the HMBC experiment. In all heteronuclear experiments, the data matrix was extended to 2,048 × 1,024 points using forward linear prediction extrapolation.

MALDI TOF MS. This study used a 4,800 Proteomic Analyzer (ABSciex), MALDI TOF/TOF (time of flight, TOF) instrument equipped with a Nd:YAG laser at a wavelength of 355 nm with <500-ps pulse and 200-Hz firing rate. External calibration was performed using an ABSciex calibration mixture. Mass accuracy was about 55 p.p.m. All measurements were performed in positive polarity. Approximately, 1,500 laser shots were accumulated for each spectrum in the MS experiments; 5,000–7,000 shots were summed for the MS/MS data acquisitions[55,56]. The tandem mass spectra reported in this study were acquired without a collision gas. Samples were dissolved in CHCl$_3$/CH$_3$OH (50:50, v/v) at a concentration of 1 mg ml^{-1}.

Matrix solution was prepared by dissolving trihydroxyacetophenone in CH$_3$OH/0.1% trifluoroacetic acid/CH$_3$CN (7:2:1, by volume) at a concentration of 75 mg ml^{-1}. One microlitre of the sample/matrix solution (1:1, v/v) was deposited on the well plate and allowed to dry at room temperature[57].

ESR and DLS studies of lipid A-containing membranes. Asymmetric liposomes were prepared assembling two independently prepared lipid monolayers. The inner one consisted of a 70/30 mol/mol mixture of 1-palmitoyl-2-oleoyl-*sn*-glycero-3-phosphoethanolamine (POPE) and 1-palmitoyl-2-oleoyl-*sn*-glycero-3-phospho-(1′-*rac*-glycerol) (POPG). In the outer one, 75% by mass of the POPE–POPG lipid mixture was substituted with HoLA (or its BTAi1Δ*shc* mutant). In some formulations, free hopanoid was also included. POPE and POPG were obtained from Avanti Polar Lipids (Birmingham, AL, USA) and used without further purification. The spin-labelled phosphatidylcholines (1-palmitoyl-2-[*n*-(4,4 dimethyloxazolidine-*N*-oxyl)]stearoyl-*sn*-glycero-3-phosphocholine, *n*-PCSL, *n* = 5, 14), used for ESR measurements, were also purchased from Avanti Polar Lipids and stored at −20 °C in ethanol solutions.

The liposome preparation procedure is schematized in Fig. 7a. The inner leaflet resulted from a W/O emulsion (the 'emulsion phase' in the Fig. 7a) which was prepared, in turn, from a lipid suspension. To prepare the lipid suspension, 80 μl of a 25-mg ml^{-1} POPE/POPG (70/30 mol/mol) stock solution in chloroform were placed in a 100-ml glass bottle. The chloroform was evaporated under nitrogen to obtain a dry, thin lipid film. After adding 4 ml of anhydrous dodecane (>99%) to reach a final lipid concentration of 0.5 mg ml^{-1}, the suspension was sonicated in a cleaning sonic bath for 45 min and left overnight at 25 °C to ensure that the lipid molecules were fully dispersed in oil before emulsifying the aqueous solution. The emulsion was prepared by adding 200 μl of an aqueous 10 mM phosphate buffer at pH = 7.4, containing 1 mM Ca^{2+}, to the lipid suspension and gently stirring the mixture with a magnetic stir bar for 1 h. Finally, the emulsion was sonicated using a tip probe for 20 min in an ice bath. Droplets' dimension distribution was checked by DLS (see Supplementary Fig. 11) to be monomodal, centred at ~130 nm. DLS analysis was performed with a set-up composed by a Photocor compact goniometer, a SMD 6000 Laser Quantum 50 mW light source operating at 5,325 Å and a PMT-120-OP/B and a correlator (Flex02-01D, Correlator.com).

The outer leaflet of the liposome was obtained from a lipid monolayer stratified at the interface between a phosphate buffer (the 'aqueous phase' in the figure) and a lipid organic mixture (the 'intermediate phase'). To prepare this organic mixture the chosen lipid A, POPE and POPG at the proper ratio were dispersed at a concentration of 0.2 mg ml^{-1} in a toluene/silicone oil (99/1 mol/mol) solution. One millilitre of this lipid dispersion was slowly placed over 0.6 ml of Ca^{2+}-containing phosphate buffer in a centrifuge tube, waiting 24 h to allow the neat stratification of the organic phase over the aqueous medium and the formation of a lipid monolayer at the interface.

Once the interface had equilibrated, 100 μl of the W/O emulsion was gently poured over the organic phase. Then the sample was centrifuged at 3,500 g for 10 min to transfer the water droplets through the interface and into the lower aqueous phase, see Fig. 7a. After centrifugation, the aqueous phase containing the liposomes was collected using a 5-ml syringe with a long stainless steel needle. Formation and dimension of obtained liposomes were assessed using DLS (Supplementary Fig. 11) and the mean hydrodynamic radius was found to be 180 and 190 nm with BTAi1Δshc and HoLA, respectively.

For ESR measurements, each liposome sample to be investigated was prepared twice, and the 5-PCSL spin-label was alternatively added to the inner (3% wt/wt on the total lipid) or outer lipid leaflet (1% wt/wt on the total lipid) by mixing appropriate amounts of a spin-label solution in ethanol (1 mg ml^{-1}) with either the POPE–POPG solution in chloroform or the lipid A dispersion in toluene/silicone oil. In a separate set of experiments, the 14-PCSL spin-label was added to the inner leaflet by using the same procedure used for the 5-PCSL spin-label. Four liposome formulations were considered (that is, eight samples were prepared): (1) symmetric POPE–POPG liposomes, used as a reference; (2) asymmetric liposomes with the external leaflet formed by a HoLA–POPE–POPG mixture and the inner leaflet formed by POPE–POPG; (3) asymmetric liposomes with the external leaflet formed by a BTAi1Δ*shc* lipid A–POPE–POPG and the inner leaflet formed by POPE–POPG; (4) asymmetric liposomes with the external leaflet

formed by the BTAi1Δ*shc* lipid A, the inner leaflet formed by POPE–POPG and the hopanoid extract, at the same mole ratio of BTAi1, added to the toluene/silicone oil mixture.

ESR spectra of 5-PCSL and 14-PCSL in the considered samples were recorded on a Elexys E-500 ESR spectrometer from Bruker (Rheinstetten, Germany) operating in the X band. Capillaries containing the samples were placed in a standard 4-mm quartz sample tube. The temperature of the sample was regulated at 30 °C and maintained constant during the measurement by blowing thermostated nitrogen gas through a quartz Dewar. Samples containing the 5-PCSL spin-label in the inner leaflet were also investigated in a temperature range spanning from 15 to 45 °C. The instrumental settings were as follows: sweep width, 120 G; resolution, 1,024 points; modulation frequency, 100 kHz; modulation amplitude, 1.0 G; time constant, 20.5 ms; sweep time, 42 s; incident power, 5.0 mW. Several scans, typically 16, were performed and averaged to improve the signal-to-noise ratio.

Construction of the BTAi1Δ*shc* mutant and complementation. To create the BTAi1Δ*shc* mutant, the complete *shc* gene was deleted and replaced by the kanamycin-resistance (KnR) gene by double crossover recombination as described below. The *KnR* gene was under the control of its own promoter and no termination sequence was introduced downstream this gene. A 2,331-bp *shc* gene fragment including 99-bp upstream and 177-bp downstream regions was amplified using the primers SHCFW (5′-CGCTACGGCCCAGTTGATTGGATTT-3′) and SHCRV (5′-TGCATCCGAAGCTCAGGACAATGA-3′) and cloned into pGEM-T easy vector (Promega Corp., Madison, WI, USA). The resulting plasmid was named pGEM-T::*shc*. The NotI fragment sized ca. 2.4 kb digested from pGEM-T::*shc* was ligated with NotI-digested pJQ200SK[58] that is not replicable in *Rhizobium* species, and which contains a counter selectable *sac*B marker, resulting in pJQ::*shc*. This pJQ::*shc* was introduced into DH5α (pKD78), which has λ Red recombinase gene controlled by *araBAD* promoter, by electroporation. The kanamycin-resistance gene was amplified from pKD4 (ref. 59) using the primers PS1 (5′-GTGTAGGCTGGAGCTGCTTC-3′) and PS2 (5′-CATATGAATATCCT CCTTAG-3′). Using the PCR product as a template, the kanamycin-resistance gene was re-amplified with two 60-bp primers PSHC1 and PSHC2, which have 40-bp linkers homologous to both bordering regions of the *shc* gene at 5′ ends of PS1 and PS2. The sequences of PSHC1 and PSHC2 are 5′-GCCCTGCAATCGACGGTG CGCGCGGCGGCGGATTGGCTGAGTGTAGGCTGGAGCTGCTTC-3′ and 5′-GTACATGCCGTAGCGGAGCATGAAGGCGCGGGACAATTCCCATATGA ATATCCTCCTTAG-3′, respectively. The consequent PCR product was introduced into DH5α (pKD78/pJQ::*shc*) and the λ Red recombinase was induced[60]. The resulting plasmid named pShc::Km was transferred into BTAi1 by triparental mating[60] and the *shc* gene replacement in sucrose-resistant clones was confirmed using PCR.

For complementation of the mutant, the complete *shc* gene was cloned downstream of the nptII promoter into the pMG103-npt2-GFP plasmid[61] harbouring a streptomycin/spectinomycin-resistance gene. For this, the streptomycin/spectinomycin-resistance gene was first liberated from pHRP315 (ref. 62) by BamHI digestion and cloned into the corresponding site of pMG103-npt2-GFP; the *shc* gene amplified using the primers SHC-BTAi1-F (5′-GGCGGAGATCTTCCC TATAGGGCGGGGTGAATTC-3′) and SHC-BTAi1-R (5′-CCGTCACTAGTCG CGCGACGGGATGGCTCGCAATG-3′) was then cloned into the BglII/SpeI sites located downstream of the nptII promoter.

Plant cultivations and symbiotic analysis. *A. evenia* seeds were surface-sterilized by immersion in sulphuric acid under shaking during 40 min. Seeds were abundantly washed with sterile distilled water and incubated overnight in sterile water. Seeds were then transferred for 1 day at 37 °C in darkness on 0.8% agar plate for germination. Plantlets were then transferred on the top of test tubes covered by aluminium paper for hydroponic culture in BNM. Plants were grown in closed mini green house in a 28 °C growth chamber with a 16-h light and 8-h dark regime and 70% humidity. Seven days after transfer, each seedling was inoculated with 1 ml of cell suspension resulting from a 5-day-old bacterial culture washed in BNM and adjusted to reach an optical density of one at 600 nm. For nodulation and nitrogen fixation kinetics at different times post inoculation (6, 8, 10, 12 and 19 days), five plants were taken to count the number of nodules on the roots and to analyse the nitrogenase activity by ARA. For this, each plant was placed into 125-ml glass vials sealed with rubber septa. Air (12.5 ml) was removed from each vial, to which 12.5 ml of acetylene was then injected. Gas samples (1 ml) were withdrawn after 3 h of incubation at 25 °C and the ethylene produced was measured using gas chromatography.

Transmission electron microscopy. Microscopic observations were performed on three to five nodules originating from different plants per condition. For this, the nodules were fixed in a 4% glutaraldehyde, 0.1 M cacodylate buffer (pH 7.2), postfixed in 1% osmium tetroxide, dehydrated using a series of acetone washes and embedded in TAAB 812 epon resin. Ultrathin sections (60 nm) were mounted on collodion carbon-coated copper grids, contrasted using uranyl acetate and lead citrate and examined at 80 kV with a TEM (Jeol 100CX II).

References

1. Ourisson, G., Rohmer, M. & Poralla, K. Prokaryotic hopanoids and other polyterpenoid sterol surrogates. *Annu. Rev. Microbiol.* **41,** 301–333 (1987).

2. Mycke, B., Narjes, F. & Michaelis, W. Bacteriohopanetetrol from chemical degradation of an oil shale kerogen. *Nature* **326,** 179–181 (1987).

3. Kannenberg, E. L., Perzl, M. & Härtner, T. The occurence of hopanoid lipids in *Bradyrhizobium* bacteria. *FEMS Microbiol. Lett.* **127,** 255–262 (1995).

4. Brocks, J. J. & Pearson, A. Building the biomarker tree of life. *Rev. Mineral. Geochem.* **59,** 233–258 (2005).

5. Sáenz, J. P., Sezgin, E., Schwille, P. & Simons, K. Functional convergence of hopanoids and sterols in membrane ordering. *Proc. Natl Acad. Sci. USA* **109,** 14236–14240 (2012).

6. Welander, P. V. *et al.* Hopanoids play a role in membrane integrity and pH homeostasis in *Rhodopseudomonas palustris* TIE-1. *J. Bacteriol.* **191,** 6145–6156 (2009).

7. Raetz, C. R. & Whitfield, C. Lipopolysaccharide endotoxins. *Annu. Rev. Biochem.* **71,** 635–700 (2002).

8. Lerouge, I. & Vanderleyden, J. O-antigen structural variation: mechanisms and possible roles in animal/plant-microbe interactions. *FEMS Microbiol. Rev.* **26,** 17–47 (2002).

9. Oldroyd, G. E., Murray, J. D., Poole, P. S. & Downie, J. A. The rules of engagement in the legume-rhizobial symbiosis. *Annu. Rev. Genet.* **45,** 119–144 (2011).

10. Masson-Boivin, C., Giraud, E., Perret, X. & Batut, J. Establishing nitrogen-fixing symbiosis with legumes: how many rhizobium recipes? *Trends Microbiol.* **17,** 458–466 (2009).

11. Olivares, J., Bedmar, E. J. & Sanjuán, J. Biological nitrogen fixation in the context of global change. *Mol. Plant Microbe Interact.* **26,** 486–494 (2013).

12. Franche, C., Lindström, K. & Elmerich, C. Nitrogen-fixing bacteria associated with leguminous and non-leguminous. *Plant Soil* **321,** 35–59 (2009).

13. Carlson, R. W., Forsberg, L. S. & Kannenberg, E. L. Lipopolysaccharides in *Rhizobium*-legume symbioses. *Subcell Biochem.* **53,** 339–386 (2010).

14. Kannenberg, E. L. & Carlson, R. W. Lipid A and O-chain modifications cause *Rhizobium* lipopolysaccharides to become hydrophobic during bacteroid development. *Mol. Microbiol.* **39,** 379–391 (2001).

15. Ferguson, G. P. *et al.* Similarity to peroxisomal-membrane protein family reveals that *Sinorhizobium* and *Brucella* BacA affect lipid-A fattyacids. *Proc. Natl Acad. Sci. USA* **101,** 5012–5501 (2004).

16. Brown, D. B., Huang, Y. C., Kannenberg, E. L., Sherrier, D. J. & Carlson, R. W. An acpXL mutant of *Rhizobium leguminosarum* bv. *phaseoli* lacks 27-hydroxyoctacosanoic acid in its lipid A and is developmentally delayed during symbiotic infection of the determinate nodulating host plant *Phaseolus vulgaris*. *J. Bacteriol.* **193,** 4766–4778 (2011).

17. Giraud, E. *et al.* Legumes symbioses: absence of Nod genes in photosynthetic bradyrhizobia. *Science* **316,** 1307–1312 (2007).

18. Silipo, A. *et al.* A unique bicyclic monosaccharide from the *Bradyrhizobium* lipopolysaccharide and its role in the molecular interaction with plants. *Angew. Chem. Int. Ed.* **50,** 12610–12612 (2011).

19. Choma, A. & Komaniecka, I. Straight and branched (ω-1)-hydroxylated very long chain fatty acids are components of *Bradyrhizobium* lipid A. *Acta Biochim. Pol.* **58,** 51–58 (2011).

20. De Castro, C., Molinaro, A., Lanzetta, R., Silipo, A. & Parrilli, M. Lipopolysaccharide structures from *Agrobacterium* and *Rhizobiaceae* species. *Carbohydr. Res.* **343,** 1924–1933 (2008).

21. Silipo, A. & Molinaro, A. in *Bacterial Lipopolysaccharides* (eds Knirel, Y. A. & Valvano, M. A.) 1–20 (Springer, 2011).

22. Komaniecka, I., Choma, A., Lindner, B. & Holst, O. The structure of a novel neutral lipid A from the lipopolysaccharide of *Bradyrhizobium elkanii* containing three mannose units in the backbone. *Chem. Eur. J.* **16,** 2922–2929 (2010).

23. Jahnke, L. L., Stan-Lotter, H., Kato, K. & Hochstein, L. I. Presence of methyl sterol and bacteriohopanepolyol in an outer-membrane preparation from *Methylococcus capsulatus* bath. *J. Gen. Microbiol.* **138,** 1759–1766 (1992).

24. Jurgens, U. J., Simonin, P. & Rohmer, M. Localization and distribution of hopanoids in membrane systems of the cyanobacterium *Synechocystis* PCC 6714. *FEMS Microbiol. Lett.* **71,** 285–288 (1992).

25. Simonin, P., Jurgens, U. J. & Rohmer, M. Bacterial triterpenoids of the hopane series from the prochlorophyte *Prochlorothrix hollandica* and their intracellular localization. *Eur. J. Biochem.* **241,** 865–871 (1996).

26. Doughty, D. M. *et al.* The RND-family transporter, HpnN, is required for hopanoid localization to the outer membrane of *Rhodopseudomonas palustris* TIE-1. *Proc. Natl Acad. Sci. USA* **108,** E1045–E1051 (2011).

27. Siedenburg, G. & Jendrossek, D. Squalene-Hopene Cyclases. *Appl. Environ. Microbiol.* **77,** 3905–3915 (2011).

28. Welander, P. V. *et al.* Identification and characterization of *Rhodopseudomonas palustris* TIE-1 hopanoid biosynthesis mutants. *Geobiology* **10,** 163–177 (2012).

29. Bosak, T., Losick, R. M. & Pearson, A. A polycyclic terpenoid that alleviates oxidative stress. *Proc. Natl Acad. Sci. USA* **105,** 6725–6729 (2008).

30. Schmerk, C. L., Bernards, M. A. & Valvano, M. A. Hopanoid production is required for low-pH tolerance, antimicrobial resistance, and motility in *Burkholderia cenocepacia*. *J. Bacteriol.* **193,** 6712–6723 (2011).

31. Malott, R. J., Steen-Kinnaird, B. R., Lee, T. D. & Speert, D. P. Identification of hopanoid biosynthesis genes involved in polymyxin resistance in *Burkholderia multivorans*. *Antimicrob. Agents Chemother.* **56,** 464–471 (2012).

32. Arrighi, J. F. *et al. Aeschynomene evenia*, a model plant for studying the molecular genetics of the Nod-independent rhizobium-legume symbiosis. *Mol. Plant Microbe Interact.* **25,** 851–861 (2012).

33. Gourion, B. *et al.* Bacterial RuBisCO is required for efficient *Bradyrhizobium Aeschynomene* symbiosis. *PLoS ONE* **6,** e21900 (2011).

34. Reid, D. E., Ferguson, B. J., Hayashi, S., Lin, Y. H. & Gresshoff, P. M. Molecular mechanisms controlling legume autoregulation of nodulation. *Ann. Bot.* **108,** 789–795 (2011).

35. Pautot, S., Frisken, B. J. & Weitz, D. A. Engineering asymmetric vesicles. *Proc. Natl Acad. Sci. USA* **100,** 10718–10721 (2003).

36. Róg, T., Pasenkiewicz-Gierula, M., Vattulainen, I. & Karttunen, M. Ordering effects of cholesterol and its analogues. *Biochim. Biophys. Acta* **1788,** 97–121 (2009).

37. Poger, D. & Mark, A. E. The relative effect of sterols and hopanoids on lipid bilayers: when comparable is not identical. *J. Phys. Chem. B* **117,** 16129–16140 (2013).

38. Pierre, O. *et al.* Peribacteroid space acidification: a marker of mature bacteroid functioning in *Medicago truncatula* nodules. *Plant Cell Environ.* **36,** 2059–2070 (2013).

39. Pauly, N. *et al.* Reactive oxygen and nitrogen species and glutathione: key players in the legume-*Rhizobium* symbiosis. *J. Exp. Bot.* **57,** 1769–1776 (2006).

40. Guefrachi, I. *et al.* in *18th Internat. Cong. Nitrogen Fixation PLN05-2* (Miyazaki, Japan, 14–18 October 2013).

41. Malott, R. J., Steen-Kinnaird, B. R., Lee, T.D. & Speert, D. P. Identification of hopanoid biosynthesis genes involved in polymyxin resistance in *Burkholderia multivorans*. *Antimicrob. Agents Chemother.* **56,** 464–471 (2012).

42. Schmerk, C. L., Bernards, M. A. & Valvano, M. A. Hopanoid production is required for low-pH tolerance, antimicrobial resistance, and motility in *Burkholderia cenocepacia*. *J. Bacteriol.* **193,** 6712–6723 (2011).

43. Vincent, J. M. *A Manual for the Practical Study of Root-Nodule Bacteria* (Blackwell Scientific Publications, 1970).

44. Podlešáková, K. *et al.* Rhizobial synthesized cytokinins contribute to but are not essential for the symbiotic interaction between photosynthetic bradyrhizobia and *Aeschynomene* legumes. *Mol. Plant Microbe Interact.* **26,** 1232–1238 (2013).

45. Westphal, O. & Jann, K. Extraction with phenol-water and further applications of the procedure. *Methods Carbohydr. Chem.* **5,** 83–91 (1965).

46. Leontein, K. & Lönngren, J. Assignment of absolute configuration of sugars by g.l.c. of their acetylated glyco-sides formed from chiral alcohols. *Methods Carbohydr. Chem.* **62,** 359–362 (1978).

47. Hakomori, S. A rapid permethylation of glycolipids and polysaccharides catalysed by methylsulfinylcarbanion in dimethylsulfoxide. *J. Biochem. (Tokyo)* **55,** 205–208 (1964).

48. Rietschel, E. T. Absolute configuration of 3-hydroxy fatty acids present in lipopolysaccharides from various bacterial groups. *Eur. J. Biochem.* **64,** 423–428 (1976).

49. Que, N. L. S., Lin, S., Cotter, R. J. & Raetz, C. R. H. Purification and mass spectrometry of six lipid A species from the bacterial endosymbiont *Rhizobium etli*. *J. Biol. Chem.* **275,** 28006–28016 (2000).

50. Bligh, E. G. & Dyer, W. J. A rapid method of total lipid extraction and purification. *Can. J. Biochem. Physiol.* **37,** 911–917 (1959).

51. Sessions, AL. *et al.* Identification and quantification of poly functionalized hopanoids by high temperature gas chromatography-mass spectrometry. *Org. Geochem.* **56,** 120–130 (2013).

52. Piantini, U., Sørensen, O. W. & Ernst, R. R. Multiple quantum filters for elucidating NMR coupling networks. *J. Am. Chem. Soc.* **104,** 6800–6801 (1982).

53. Rance, M. *et al.* Improved spectral resolution in COSY 1H NMR spectra of proteins via double quantum filtering. *Biochem. Biophys. Res. Commun.* **117,** 479–485 (1983).

54. States, D. J., Haberkorn, R. A. & Ruben, D. J. A two-dimensional nuclear overhauser experiment with pure absorption phase in four quadrants. *J. Magn. Reson.* **48,** 286–292 (1982).

55. Sturiale, L. *et al.* Reflectron MALDI TOF and MALDI TOF/TOF mass spectrometry reveal novel structural details of native lipooligosaccharides. *J. Mass Spectrom.* **46,** 1135–1142 (2011).

56. Spina, E. *et al.* New fragmentation mechanisms in matrix-assisted laser desorption/ionization time-of-flight/time-of-flight tandem mass spectrometry of carbohydrates. *Rapid Commun. Mass Spectrom.* **18,** 392–398 (2004).

57. Leone, S. *et al.* Detailed characterization of the lipid A fraction from the nonpathogen *Acinetobacter radioresistens* strain S13. *J. Lipid Res.* **48,** 1045–1051 (2007).

58. Quandt, J. & Hynes, M. F. Versatile suicide vectors which allow direct selection for gene replacement in gram-negative bacteria. *Gene* **127,** 15–21 (1993).

59. Datsenko, K. A. & Wanner, B. L. One-step inactivation of chromosomal genes in *Escherichia coli* K-12 using PCR products. *Proc. Natl Acad. Sci. USA* **97,** 6640–6645 (2000).

60. Lee, H. I., Lee, J. H., Park, K. H., Sangurdekar, D. & Chang, W. S. Effect of soybean coumestrol on *Bradyrhizobium japonicum* nodulation ability, biofilm formation, and transcriptional profile. *Appl. Environ. Microbiol.* **78,** 2896–2903 (2012).

61. Bonaldi, K. *et al.* The Nod factor-independent symbiotic signaling pathway: development of *Agrobacterium rhizogenes*-mediated transformation for the legume *Aeschynomene indica. Mol. Plant Microbe Interact.* **23,** 1537–1544 (2010).

62. Parales, R.E & Harwood, C.S. Construction and use of a new broad-host-range lacZ transcriptional fusion vector, pHRP309, for gram-bacteria. *Gene* **133,** 23–30 (1993).

63. Gourion, B., Francez-Charlot, A. & Vorholt, J. A. PhyR is involved in the general stress response of *Methylobacterium extorquens* AM1. *J. Bacteriol.* **190,** 1027–1035 (2008).

Acknowledgements

Author contributions

A.S., E.G. and A.M. conceived the study, designed and executed the research and wrote the manuscript. All the authors contributed to execute the research, to analyse the data and to write the manuscript.

Additional information

Supplementary Information accompanies this paper at http://www.nature.com/naturecommunications

Competing financial interests: The authors declare no competing financial interests.

Reprints and permission information is available online at http://npg.nature.com/reprintsandpermissions/
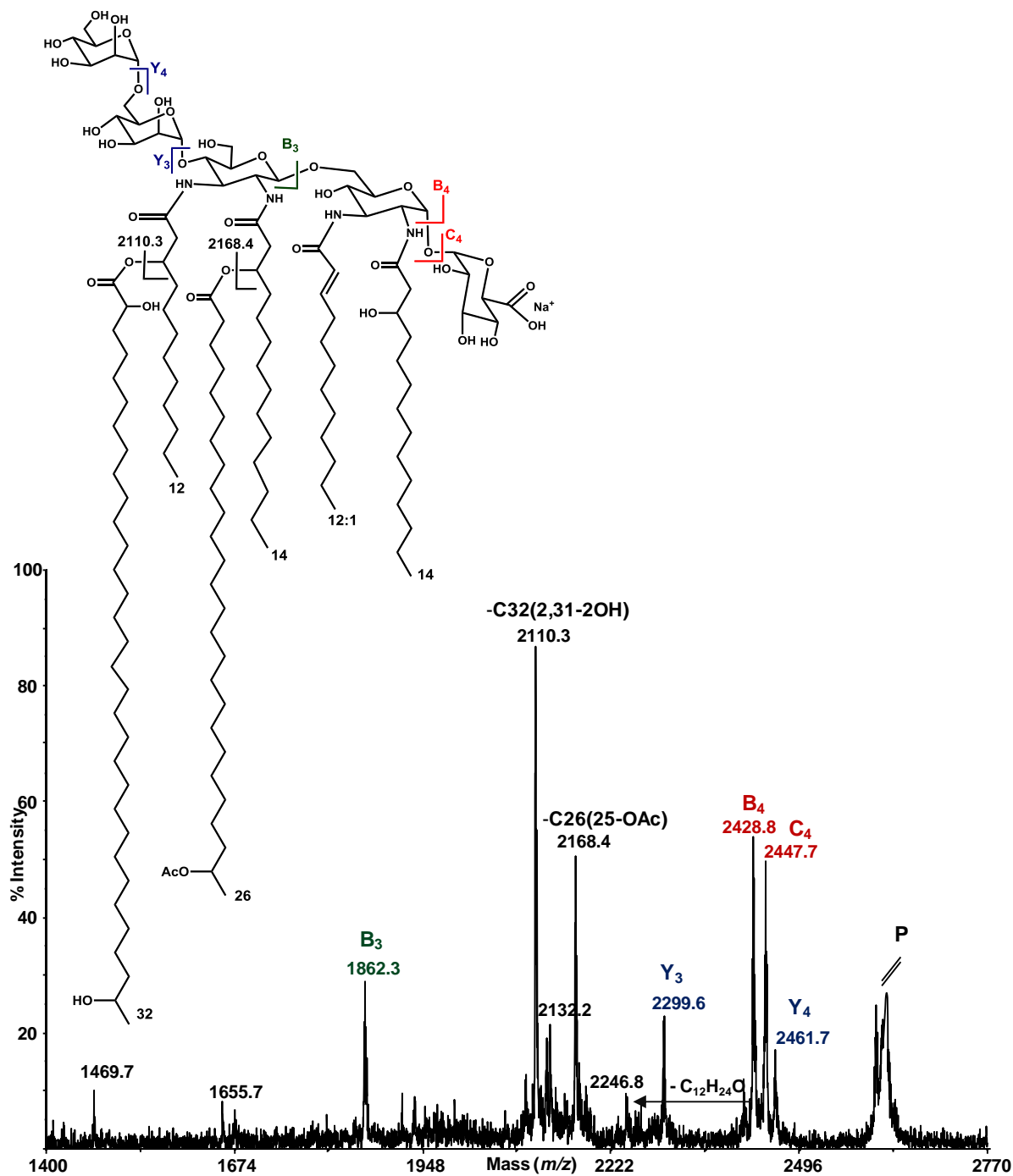
How to cite this article: Silipo, A. *et al.* Covalently linked hopanoid-lipid A improves outer-membrane resistance of a *Bradyrhizobium* symbiont of legumes. *Nat. Commun.* 5:5106 doi: 10.1038/ncomms6106 (2014).
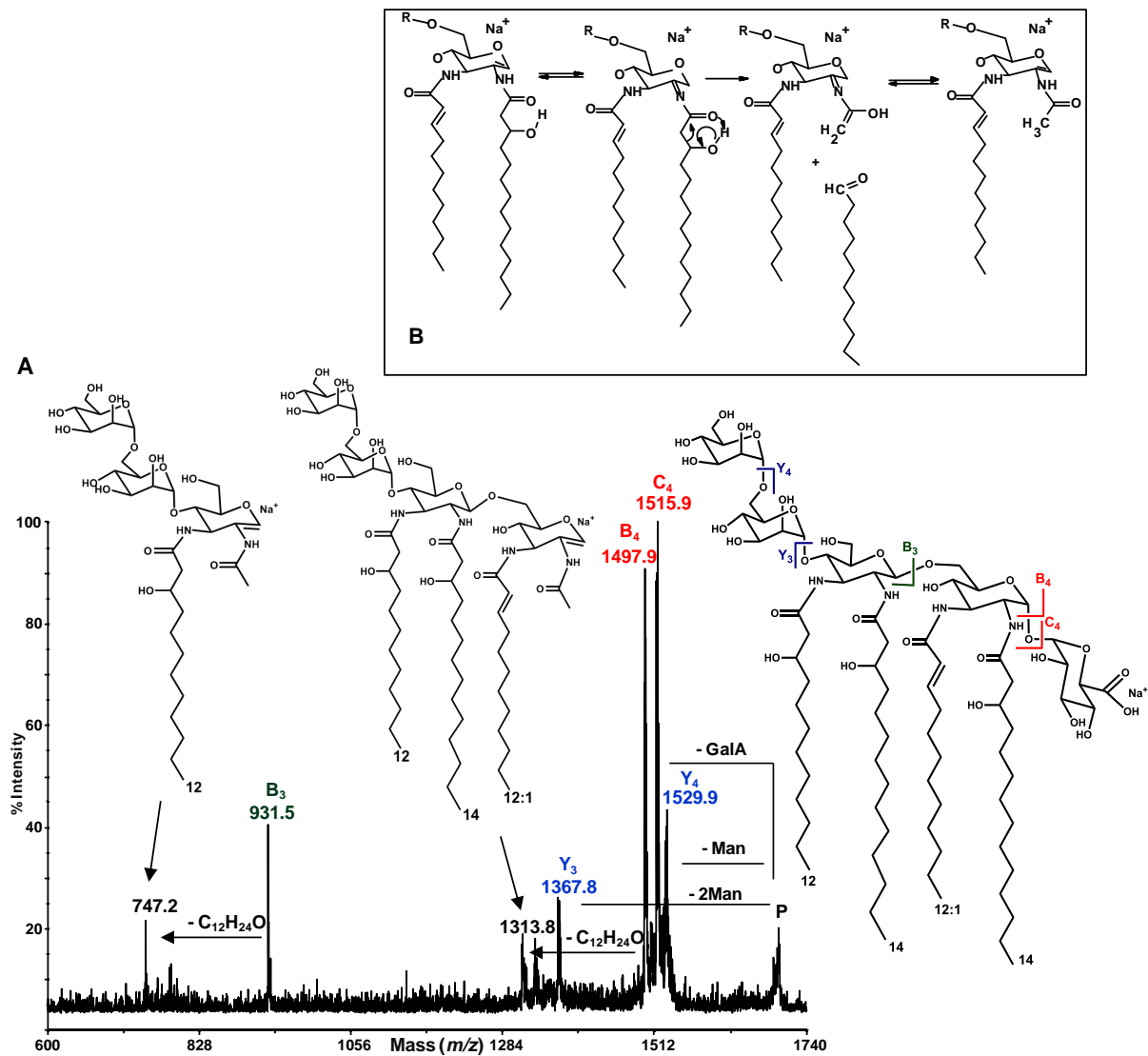
**Supplementary Figure 1: MS² of *O*-deacylated lipid A.**

a. MALDI TOF/TOF MS² analysis of the *O*-deacylated lipid A from *Bradyrhizobium*BTAi1, whose structure has been also sketched. (GalA, Galacturonic acid; Man, Mannose)

b. Losses of $C_{12}H_{24}O$ from B ions refer to a six point molecular rearrangement involving the free 3-OH group on the 14:0 acyl chains. P: parent ion at *m/z* 1691.76.

Supplementary Figure 2: MS^2 on intact penta-acylated lipid A. MALDI TOF/TOF MS^2 analysis of the penta-acylated lipid A species at *m/z* 2128.42. Loss of $C_{12}H_{24}O$ from B_4 ion is outlined in the inset of Fig. 1. P: parent ion.

Supplementary Figure 3: MS² on intact hexa-acylated lipid A. MALDI TOF/TOF MS²
analysis of the hexa-acylated lipid A species at m/z 2622.96. Loss of $C_{12}H_{24}O$ from B_4 ion is
outlined in the inset of Fig. 1. P: parent ion.
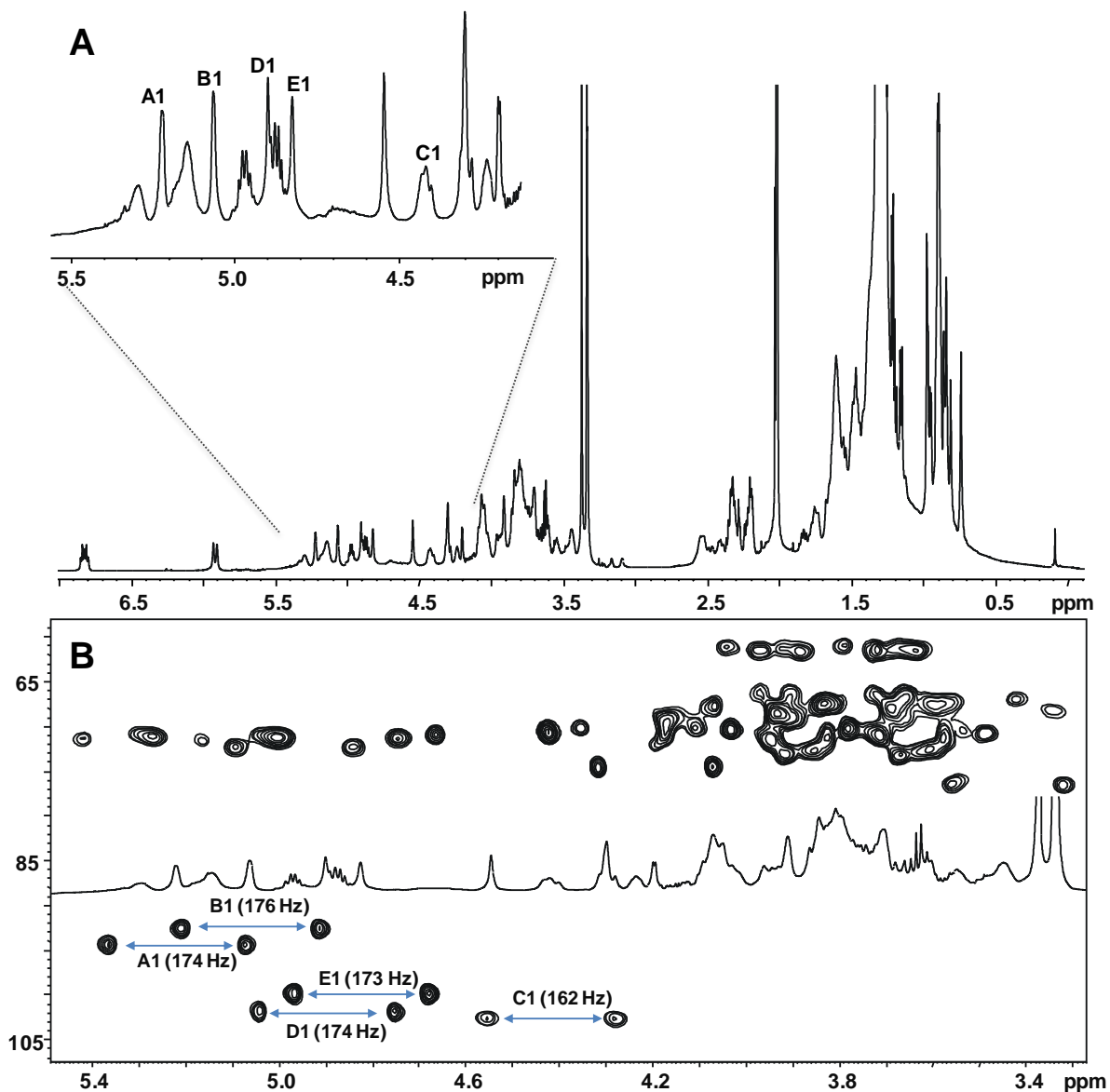
Supplementary Figure 4: NMR on intact lipid A.

a. ^{1}H NMR spectrum of the lipid A from *Bradyrhizobium*BTAi1. Anomeric signals in the inset are as attributed in Supplementary Table 2.

b. *F2-coupled* HSQC. Zoom of the anomeric region of the *F2-coupled* HSQC spectrum in which the diagnostic heteronuclearanomeric constants are shown. This experiment allowed us to define the anomeric configuration of the sugar units.
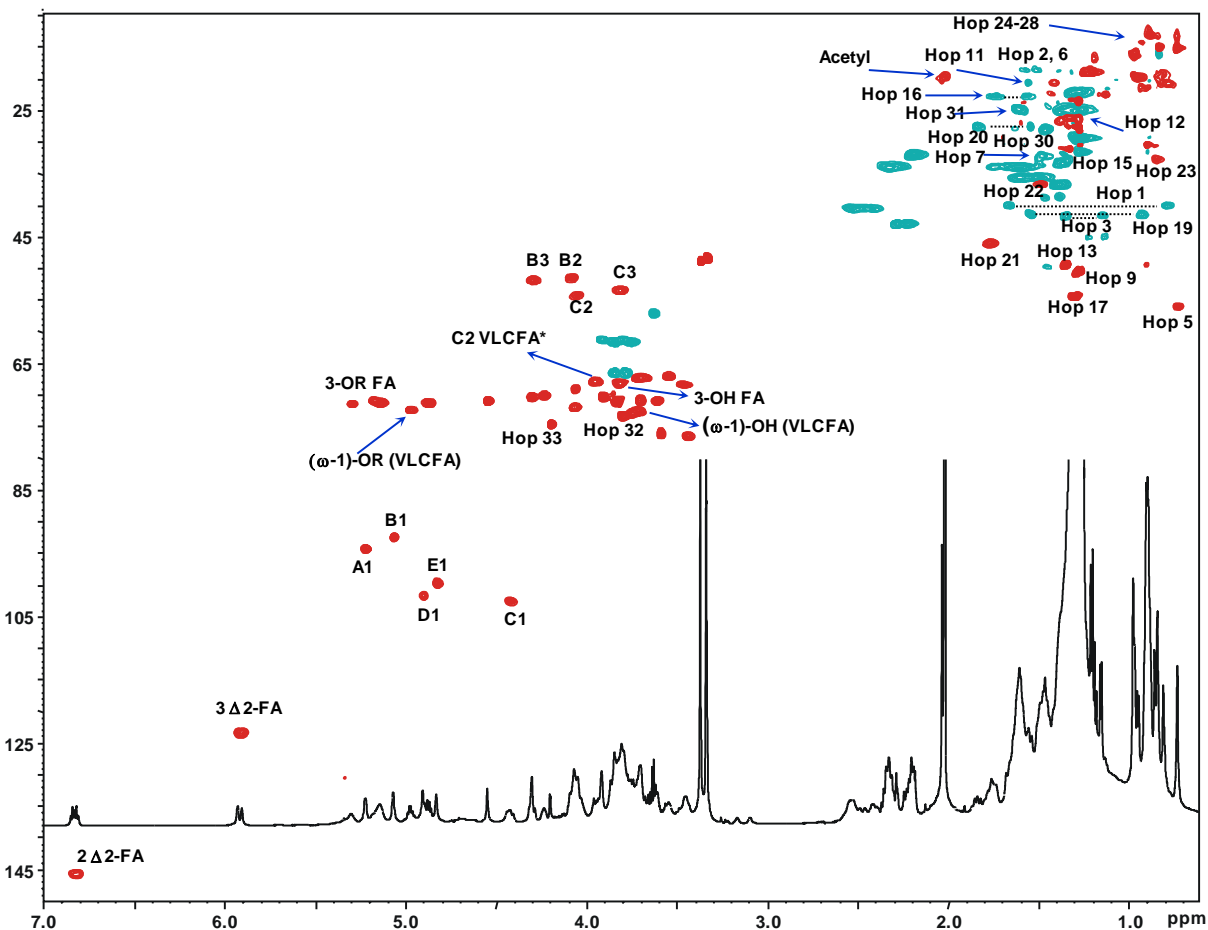
Supplementary Figure 5: HSQC NMR spectrum of *Bradyrhizobium* lipid A.
HSQC spectrum of the lipid A from *Bradyrhizobium* BTAi1. Key signals from the sugar backbone and lipid moieties are indicated. Numbering of hopanoid is as reported in Fig. 1 and Supplementary Table 2. *C2 VLCFA refers to the long chain fatty acids hydroxylated at position 2 (Supplementary Table 1-2)
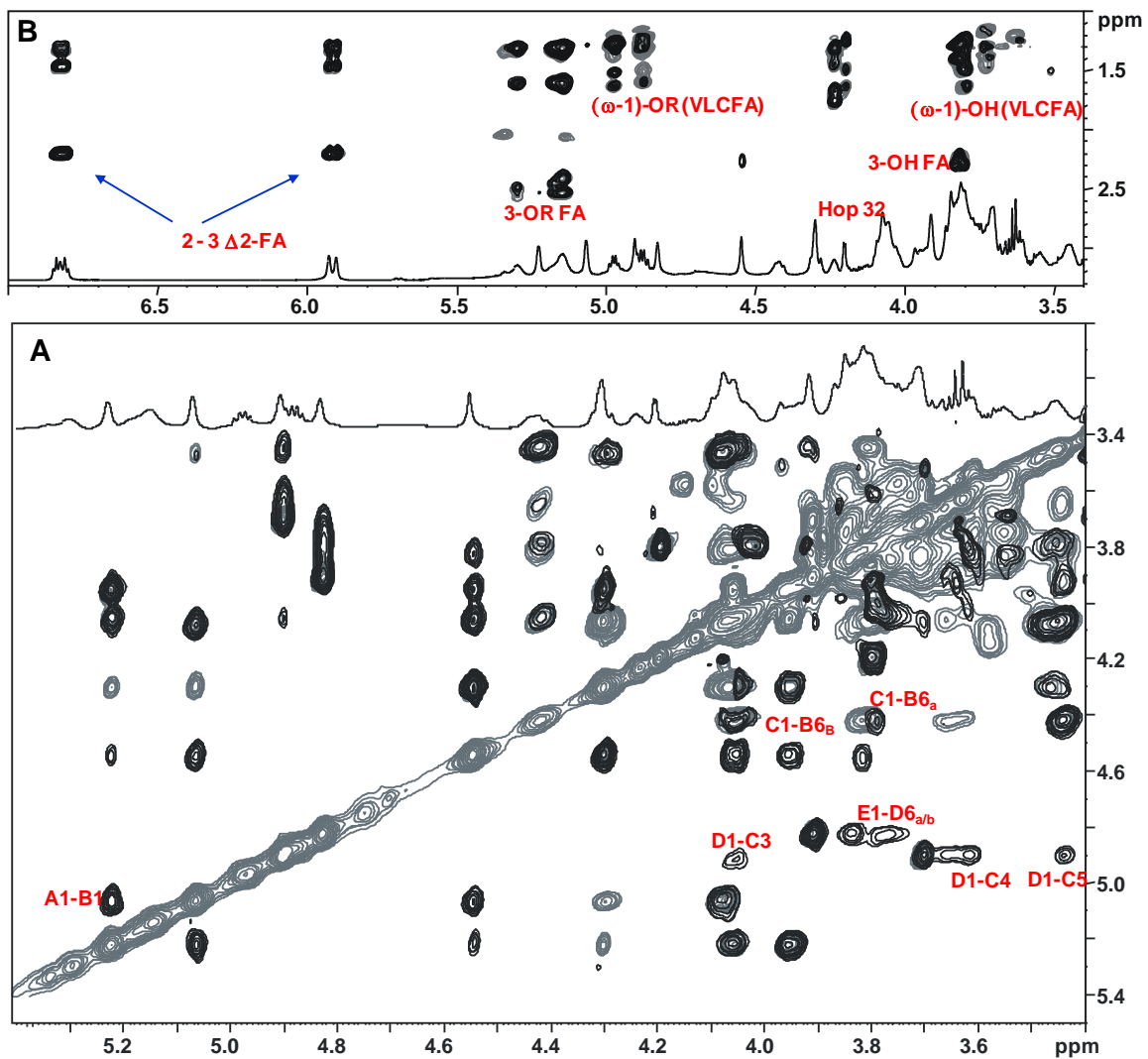
Supplementary Figure 6: Definition of the sugar skeleton and of the acylation pattern.
a. Zoom of ROESY (black) and TOCSY (grey) spectra related to the sugar resonances. The main *inter*-residual correlations used to assign, together with the HMBC spectrum, the sugar backbone, were indicated. Letters are as reported in Supplementary Table 2.
b. ROESY (black) and TOCSY (grey) spectra of the lipid A from *Bradyrhizobium*BTAi1; the differently hydroxilated lipid moieties have been indicated (Supplementary Table 2).
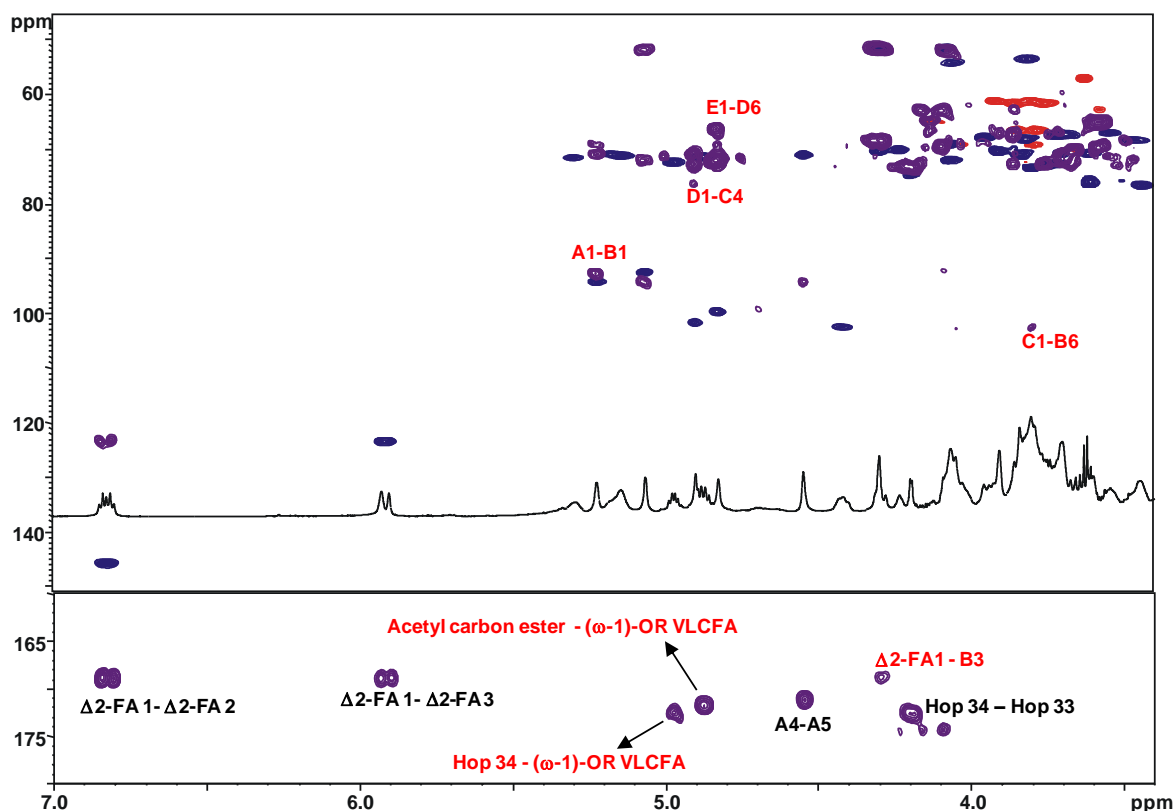
Supplementary Figure 7: HSQC and HMBC NMR spectra of *Bradyrhizobium* lipid A.
HSQC (blue and red) and HMBC (violet) spectra; the key *inter*-residual long range
correlations involving sugar moieties (**A-D**) and the unsaturated fatty acid (**Δ2-FA1 - B3**) are
indicated in red; letters are as in Supplementary Table 2. The substitution pattern of the two
O-acylated VLCFA were identified by the long-range correlations (red coloured) of: i) the
acetyl carbon ester with the ω−1 position of a VLCFA (acetyl carbon ester - (ω-1) OR LCFA)
and ii) the carbon ester at position 34 of the hopanoid with the ω−1 position of a second
VLCFA (Hop 34- (ω-1) OR LCFA). Letters are as indicated in Supplementary Table2.
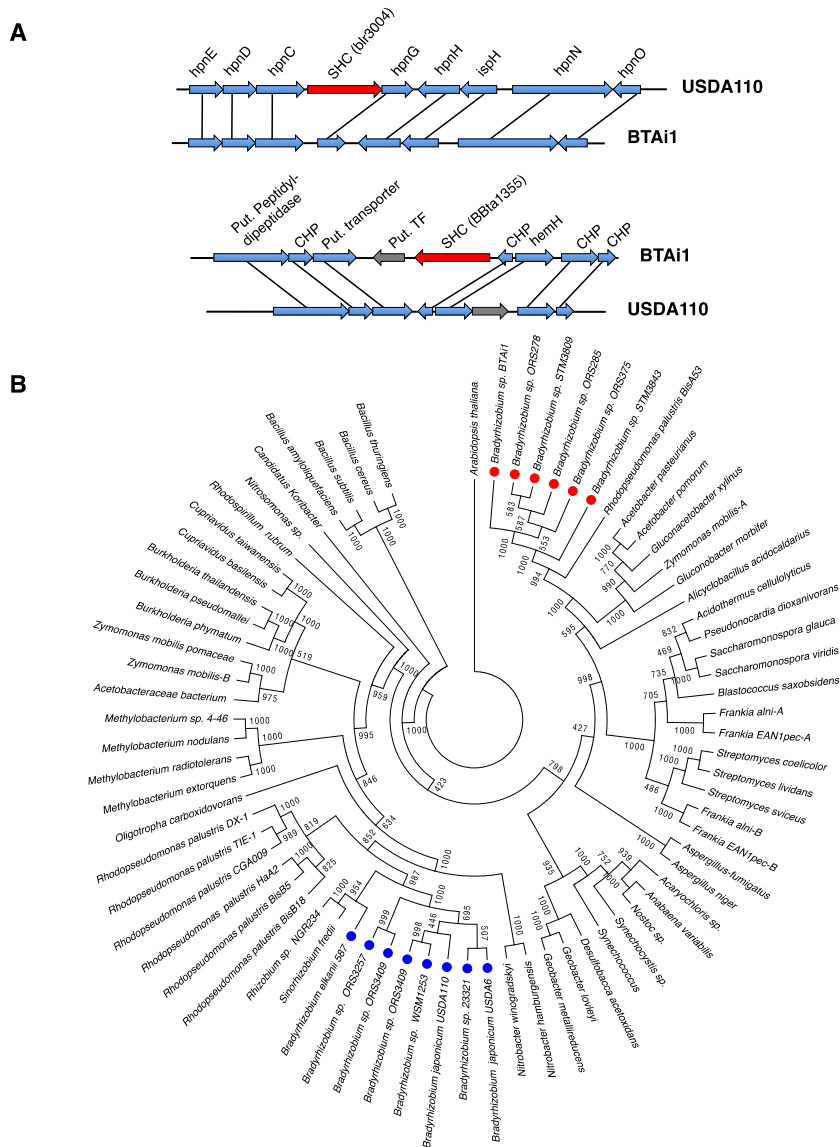
Supplementary Figure 8. Two distinct Shc identified in *Bradyrhizobium* sp. strains.
a. Genetic organization of the genes surrounding the *shc* gene in *Bradyrhizobium diazoefficiens*USDA110 and *Bradyrhizobium* sp. BTAi1. The genes annotated *hpn* were shown to be involved in hopanoid biosynthesis in *R. palustris* TIE1. In red, the *shc* gene; in blue, the genes that are found in synteny in both bacteria and in grey, genes specific to each bacteria. CHP, conserved hypothetical protein; TF, transcriptional factor.
b. Phylogenetic tree of Shc identified in various sequenced genomes. The tree was built by neighbour-joining from a matrix corrected by the Kimura-2 parameter method. Numbers at nodes are bootstrap values based on 1000 resamplings. The photosynthetic and non-photosynthetic *Bradyrhizobium* strains are marked respectively by a red and a blue circle.
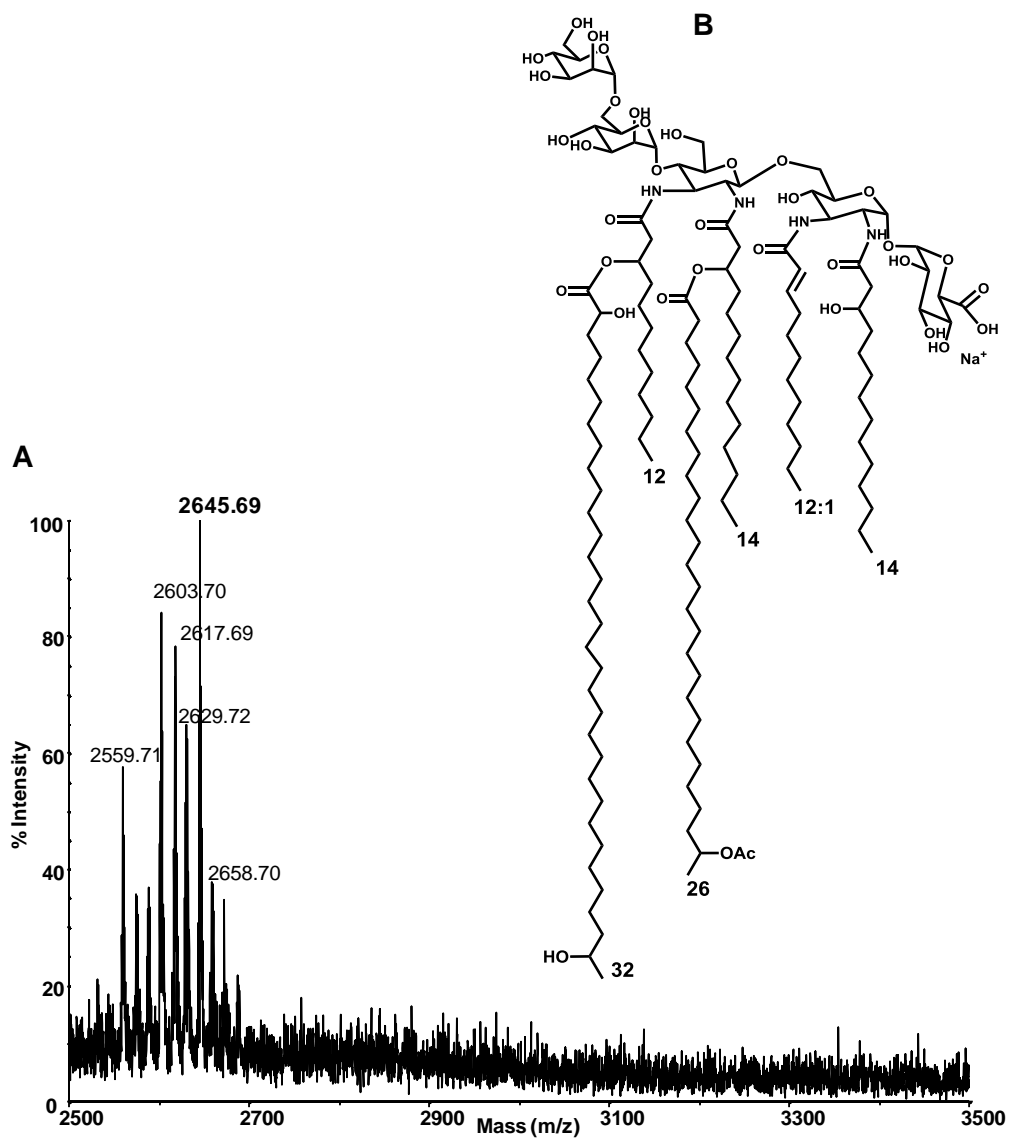
Supplementary Figure 9: Structure of the lipid A from *Bradyrhizobium*BTAi1Δshc

a. Reflectron MALDI TOF mass spectrum of the lipid A from *Bradyrhizobium*BTAi1Δ*shc* showing the complete absence of the HoLA species. All the molecular ions were detected as di-sodiated ion adducts.

b. Structure of the main lipid A species of *Bradyrhizobium*BTAi1Δ*shc* at *m/z* 2645.69.
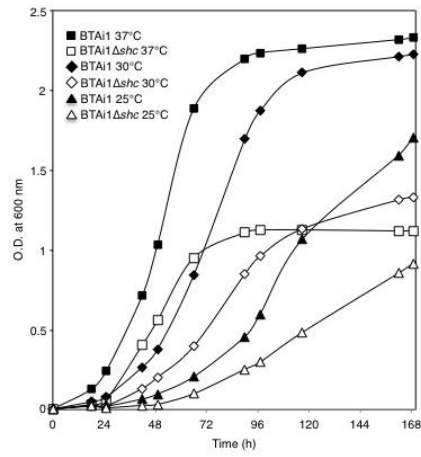
Supplementary Figure 10: Effect of the temperature on the growth.
Effect of the temperature on the growth of BTAi1 and BTAi1Δ*shc* strains cultivated in rich medium.
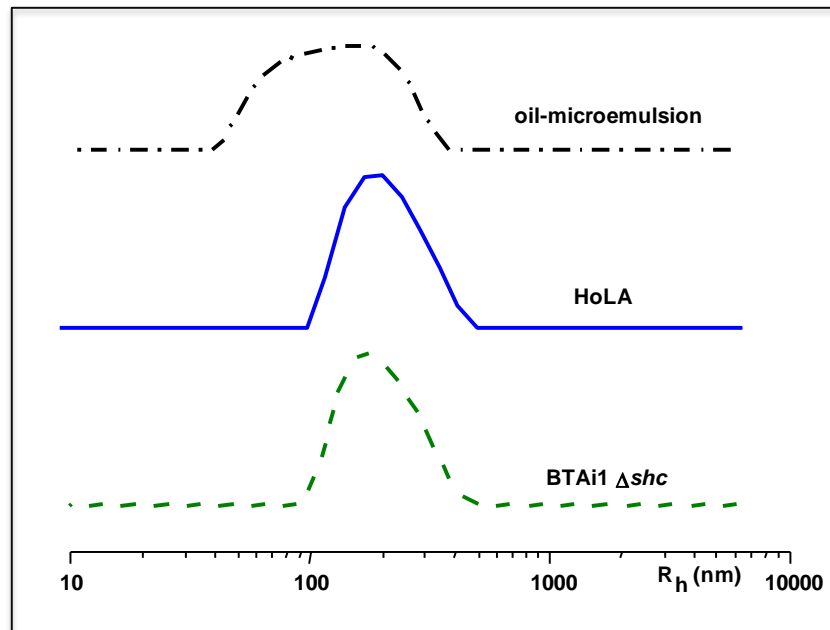
Supplementary Figure 11: DLS measurements of asymmetric liposomes.
Size distribution of emulsion and asymmetric liposomes obtained from DLS measurements performed at 90°.
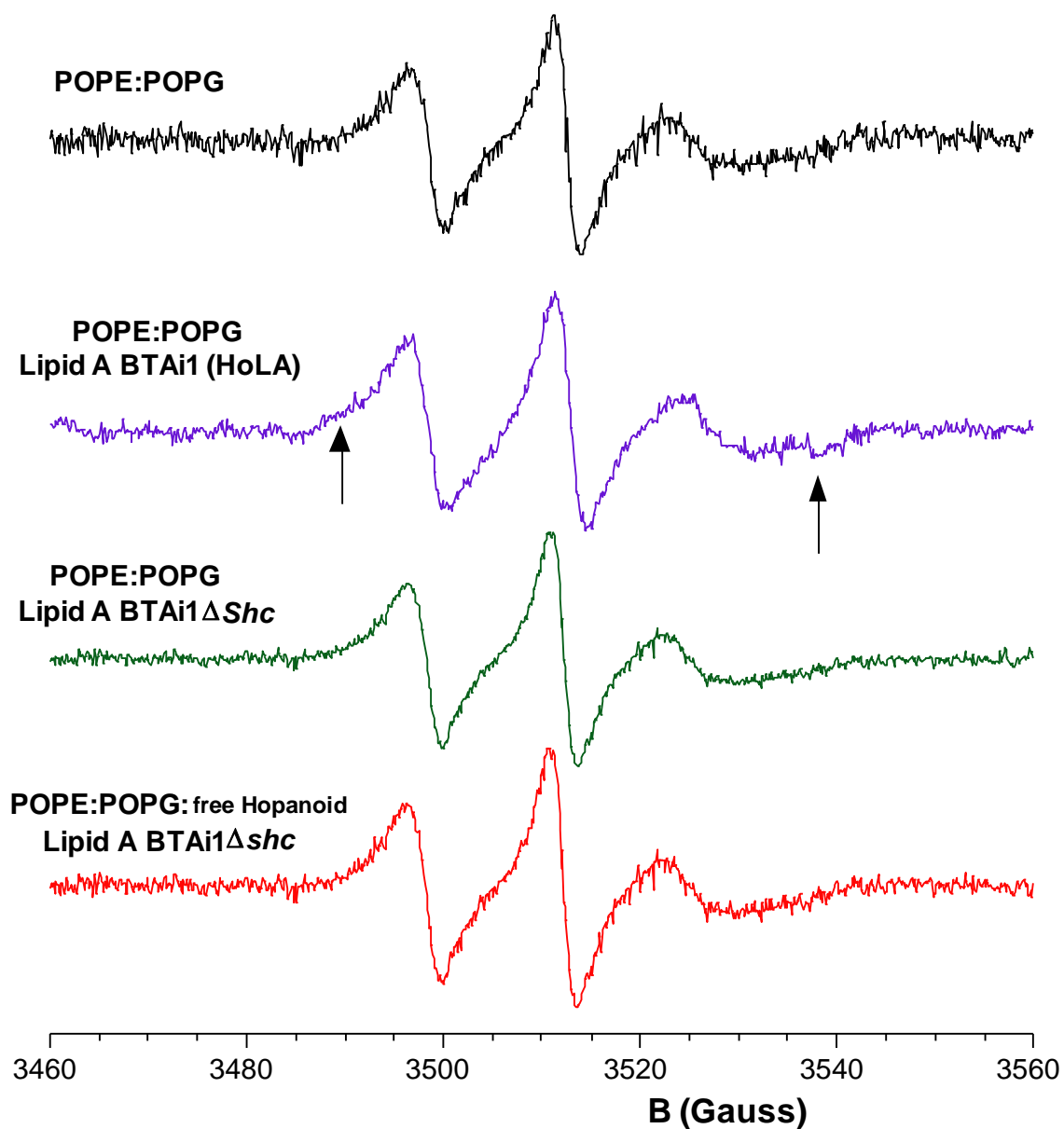
Supplementary Figure 12. EPR spectra of 14-PCSL in the inner leaflet of the asymmetric liposomes.
Components of the outer leaflet are specified in the figure. In all cases, the inner leaflet is composed by a POPE/POPG mixture. The arrows highlight the low-field shoulder and the high field minimum indicative of a second, more motionally restricted, component.
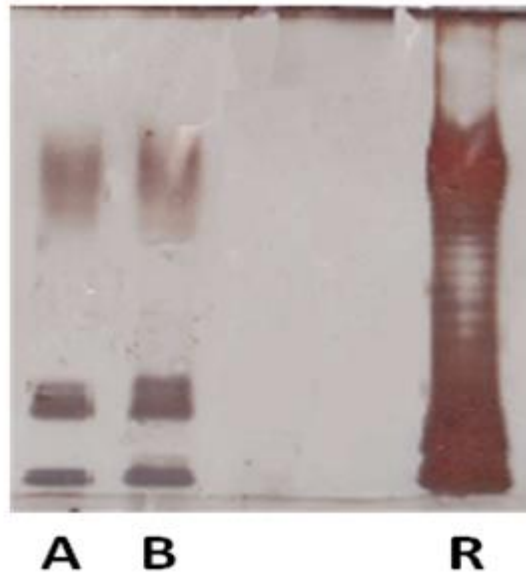
Supplementary figure 13. SDS-PAGE.
SDS PAGE of the extracted and purified LPS from *Bradyrhizobium*BTAi1 (Lane A) and *Bradyrhizobium* BTAi1Δ*shc* (Lane B); the LPS of *E. Coli* (R) was used as reference.
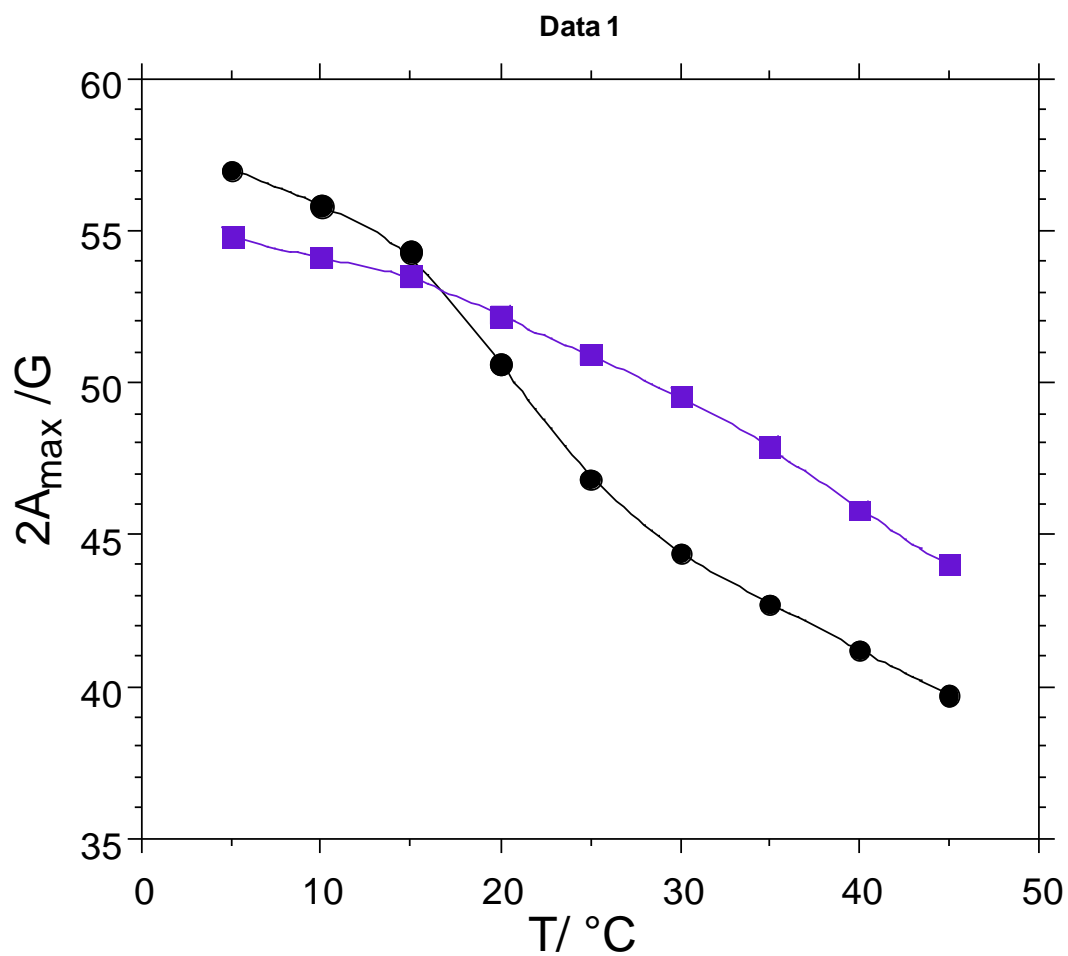
Supplementary figure 14. Outer hyperfine splitting, $2A_{max}$, of 5-PCSL in the outer leaflet of the asymmetric liposomes.
Components of the outer leaflet are POPE/POPG (black circles) or POPE/POPG/HoLA (violet squares), reported as a function of the temperature. In all cases, the inner leaflet is composed by a POPE/POPG mixture.

Supplementary Table 1: Sugar and fatty acid composition of *Bradyrhizobium* BTAi1 lipid A.

Sugar residues
GlcN3N
GalA
Man
Fatty acid residues
12:0(3-OH)
14:0(3-OH)
Δ2-12:1
12:0
26:0(25-OH)
28:0(27-OH)
30:0(29-OH)
30:0(2,29-2OH)
31:0(30-OH)
32:0(31-OH)
32:0(2,31-2OH)
33:0(2,32-2OH)
Hopanoic acid
Tetrakis-homo-hopane-32,33-diolic acid $C_{34}H_{58}O_4$

Supplementary Table 2. ^{1}H /^{13}C chemical shift values of relevant signals of lipid A from *Bradyrhizobium* BTAi1. Numbering of hopanoid signals is as reported in figure 1.

a) **Sugar backbone:**

Chemical shift δ (^{1}H/^{13}C)						
Unit	1	2	3	4	5	6
A	5.22	3.95	4.05	4.29	4.54	/
1−α−GalA	94.3	67.8	71.9	70.3	70.9	171.0
B	5.06	4.08	4.29	3.46	4.07	3.79/3.90
6−α−GlcN3N	92.4	51.3	51.8	68.3	71.9	69.1
C	4.41	3.8	4.07	3.65	3.44	3.91/3.80
4−β−GlcN3N	102.5	53.4	54.1	75.2	76.5	61.1
D	4.89	3.70	3.60	3.55	3.72	3.84/3.78
6−α−Man	101.8	70.7	70.7	67.0	72.5	66.5
E	4.82	3.90	3.83	3.71	3.79	3.84/3.76
t−α−Man	99.7	70.2	71.1	67.1	73.3	61.5

b) Fatty acid signals:

Fatty acid	α_1/α_2	β	γ	$(CH_2)_n$	CH_3
I–(3–OR) fatty acid	2.48/2.55	5.29	1.6	1.31	0.88
	40.63	71.32	34.08	28.6	13.0
II–(3–OR) fatty acid	2.40/2.53	5.14	1.59	1.31	0.88
	40.57	71.2	35.08	28.6	13.9
	α_1/α_2	β	γ	$(CH_2)_n$	CH_3
3–OH fatty acid	2.23/2.29	3.83	1.4	1.27	0.94
	42.9	68.1	36.6	28.6	
Acetyl group	CH_3	2.03	C=O		
		19.94	171.5		
Unsaturated fatty acid Δ2-FA	**2 Δ2-FA**	**3 Δ2-FA**			
	6.80	5.96			
	145.6	123.2			
VLCFA	ω–2	ω–1	ω		
verylong chain (ω-1)–OH	1.4/1.38	3.72	1.15		
	38.6	67.3	22.4		
Istverylong chain (ω-1)–OR	1.51/1.62	4.97	1.24		
Esterified by the hopanoic acid	35.6	72.3	19.1		
IIndverylong chain (ω-1)–OR	1.59/1.50	4.87	1.20		
Esterified by an acetyl group	35.5	71.3	19.0		

c) Hopanoid signals

Relevant hopanoid signals		
Position	^{1}H	^{13}C
1	0.789/1.66	39.87
2	1.50/1.38	18.6
3	1.348/1.14	41.7
4	-----	32.7
5	0.73	56.01
6	1.50/1.38	18.6
7	1.48	32.0
8	-----	41.9
9	1.28	50.37
10	-----	37.3
11	1.55	20.5
12	1.45/1.40	23.9
13	1.35	49.31
14	-----	41.7
15	1.36	33.1
16	1.55/1.73	22.67
17	1.30	54.4
18	-----	44.3
19	0.927/1.544	41.37
20	1.83/1.54	27.6
21	1.76	46.14
22	1.60	35.5
23	0.89	30.26
24	0.79	20.8
25	0.82	15.16
26	0.96	16.0
27	0.98	16.3
28	0.73	15.6
29	0.94	19.58
30	1.45	27.96
31	1.60	24.7
32	3.79	73.26
33	4.19	74.4
34	-----	172.3

Supplementary Table 3: Composition of ions present in Fig. 1c

Observed ions (*m/z*)	MS/MS assignments
3135.4	MNa^+
2972.7	Y_4
2959.2	C_4
2941.2	B_4
2811.1	Y_3
2757.6	$B_4 - C_{12}H_{24}O$ (see scheme in Supplementary Fig.1)
2681.0	MNa^+ - C26:0(25-OAc)
2604.8	MNa^+ - hopandiolic acid
2375.8	B_3
2111.3	MNa^+ - C32:0(2,31-2OH) - hopandiolic acid
1658.3	MNa^+ - C32:0(2,31-2OH) - hopandiolic acid - C26:0(25-OAc)

Supplementary Table 4 Values of the outer hyperfine coupling constant evaluated from the ESR spectra of 5-PCSL in outer and inner leaflet of the indicated asymmetric bilayers.

	$2A_{max}$/G ($\pm$ 0.5)
outer leaflet POPE/POPG	44.4
innerleafletPOPE/POPG	44.6
outerleafletLipidABtAi/POPE/POPG	49.5
innerleafletPOPE/POPG	52.3
outerleafletLipidA BtAi-1Shc/POPE/POPG	46.8
innerleafletPOPE/POPG	46.3
outer leaflet LipidA BtAi-1Shc/hopanoid/POPE/POPG	50.1
innerleafletPOPE/POPG	45.2

Supplementary Notes

Supplementary Note 1

Characterization of lipid A from the atomic to the supramolecular level.

Compositional analysis of the lipid A furnished the chemical constituents of the lipid A, fundamental to unveil the information provided from the other techniques. Indeed, MS gave us a picture of the molecular species composing the lipid A blend, providing important clues like the nature of heterogeneity, molecular masses, the number, the distribution and the location of lipid chains. NMR spectroscopy was used, in parallel, to unambiguously identify, at atomic resolution, lipid A constituents, for instance to define the sugar skeleton, to characterise and locate the lipids components. Once defined the structure of the lipid A, ESR and DLS techniques, performed on reconstituted bacterial membranes, were used to investigate the micro- and meso-structural properties of these systems, to monitor the characteristic of the membrane regions, such as permeability and stability, and finally to relate these supramolecular properties of the bacterial cell envelope to the molecular structure of the lipid A.

Supplementary Note 2

Isolation, purification and characterization of lipid A from *Bradyrhizobium*

Dried cells from *Bradyrhizobium*BTAi1 strain were collected and the LPS extraction was performed with hot phenol/water. The SDS-PAGE analysis of the LPS showed that BTAi1 LPS was of the smooth type, as indicated by the presence of high molecular-mass species in the upper part of the gel (Supporting Figure 13). A mild acid hydrolysis was performed on the LPS fraction to isolate the lipid A. Chemical analysis performed on the lipid A showed the presence of 6-linked and terminal mannose (Man), 6-substituted and 4-substituted 2,3-diamino-2,3-dideoxy-glucose (DAG) and terminal galacturonic acid (GalA), and, as fatty acids, 12:0(3-OH), 14:0(3-OH), Δ2-12:1, Δ2-14:1, 12:0, and the VLCFA26:0(25-OH), 28:0(27-OH), 30:0(29-OH), 30:0(2,29-2OH), 31:0(30-OH), 32:0(31-OH) (Supplementary Table 1). Usually, the Δ2-unsaturated fatty acids represent artefacts originating from β-elimination of 3-OH fatty acids, occurring during fatty acid analysis, however, NMR and MS data confirmed that Δ2-12:1 was present as component of the lipid A (see below). In addition,

Lipid A GC-MS analysis also showed the presence of hopanoids. In particular, GC-MS data showed the presence of hopanediolic acid (Fig. 1a).

Supplementary Note 3

MALDI TOF MS and MS/MS analysis of lipid A.

MS and MS/MS analysis on the *O*-deacylated lipid A were performed; the main molecular ion [M+Na$^+$] at *m/z*1691.76,present in the MALDI TOF spectrum (data not shown), was found consistent with a tetra-acylated oligosaccharide backbone (two DAG, two Man, one GalA) connected with two 14:0(3-OH), one 12:0(3-OH) and one unsaturated 12:1. The detailed structure of this species was accurately defined by MALDI TOF/TOF MS^2 analysis (Supplementary Fig. 1). All the fragment ions accounting for the cleavage of the glycosidic bonds (as sketched in the *O*-deacylated lipid A structure also present in Supplementary Fig. 1, pointed to a saccharide sequence on the DAG backbone in fully accordance with the NMR data. Actually, Y$_4$ (*m/z*1529.9) and Y$_3$ ions (*m/z*1367.8) corresponded to the loss of one and two Man residues respectively from the non-reducing oligosaccharide end. The fragmentation spectrum also showed a very informative peak at *m/z*931.5identified as a B$_3$ ion generated from the rupture of the glycosidic linkage between the two aminosugars and consisting in two Man and one DAG N-substituted by a 14:0(3-OH) and a 12:0(3-OH) acyl moiety. A subsequent rearrangement of B$_3$ ion, promoted by the free 3-OH group on the14:0 (as described in the inset in Supplementary Fig. 1), resulted in the loss of 184mass units (C$_{12}$H$_{24}$O), giving the ion at *m/z*747.2 (Supplementary Fig.1). This fragmentation was very helpful to establish that the primary acylated 14:0(3-OH) is sitting at position 2 of the distal DAG. In addition, fragments at *m/z*1515.9, 1497.9 and 1313.8were informative of the location of primary acyl chains on the proximal DAG residue. In detail, the loss of the reducing terminal GalA gave B- and C-type ions as very abundant species at *m/z* 1515.9 (C$_4$) and 1497.9(B$_4$). Further fragmentation of B$_4$, analogously to B$_3$ ion, originated the peak at *m/z*1313.8(loss of C$_{12}$H$_{24}$O, see Supplementary Fig. 1 inset). All these results proved that the primary 14:0(3-OH) is located at position 2 of the DAG and, as a consequence, the unsaturated acyl moiety 12:1 is *N*-linked at position 3.

The positive ion MALDI spectrum performed on the intact lipid A (Fig. 1b) exhibited a heterogeneous mixture of ion peaks (present as Na$^+$ adducts) belonging to three families of lipid A species which differed in the acylation pattern at the saccharide skeleton; for each series, whose major components were found at *m/z*2128.42, 2594.93 and 3107.34, the mass differences between neighbouring ions were due to the different lengths and/or substitution

pattern of the ester-linked acyl chains (Supplementary Table 1). The lowest molecular mass peak at m/z2128.42was found compatible with a penta-acylated species with two 14:0(3-OH), one 12:0(3-OH), one 12:1 and one 26:0(25-OAc); it is worth to note that no additional peaks were observed in the mass-range nearby the penta-acyl lipid A moiety, thus indicating that no heterogeneity, neither in the length nor in the substitution pattern, is due to the ester linked 26:0(25-OAc).The positive ion MS/MS spectrum of this parent ion (m/z2128.42) reported in Supplementary Fig.2, showed, besides the ion series generated from the cleavage of the glycosidic linkages (i.e. Y_4 at m/z1966.6, C_4 at m/z1952.5, B_4 at m/z1934.6, and Y_3 at m/z1804.5) also a significant ion peak at m/z1674.1, corresponding to a tetra-acylated fragment devoid of the VLCFA 26:0(25-OAc). Moreover, the overall fragmentation pattern allowed to ascertaining the exact position of this secondary O-substitution: peaks at m/z1934.6 and 1367.8were both referred to B-type ions (B_4 and B_3 respectively) originated from the glycosidic linkage cleavages *via* β-elimination. In particular B_3 ion at m/z1367.8, consistent with a tri-acylated lipid A fragment having 14:0(3-OH) and 12:0(3-OH) as primary and 26:0(25-OAc) as secondary acyl substituents, provided a clear evidence that this latter moiety was bound to the non-reducing DAG residue. Since, unlike the B_4 ion flanking peak at m/z 1750.3due to the meaningful loss of 184mass units ($C_{12}H_{24}O$), no additional signal was found in the mass-range below B_3, it could be reasonably inferred that the 3-OH substitution on 14:0 by the secondary acyl chain prevents the molecular rearrangement leading to that fragmentation, thus suggesting that the VLCFA 26:0(25-OAc) was located on the 14:0(3-OH) occurring at position 2 of the distal DAG.

The MS/MS analysis on the parent ion at m/z2622.96(Supplementary Fig.3) showed this species corresponding to a hexa-acylated lipid A sharing with the penta-acylated ion at m/z 2128.42the same structure plus an additional secondary VLCFA recognized as 32:0(2,31-2OH). In this case, B_3 ion found at m/z1862.3, was consistent with the following composition: one residue of GlcN3N, two residues of Man, one 14:0(3-OH), 12:0(3-OH), 26:0(25-OAc), 32:0(2,31-2OH), allowing us to disclose a peculiar lipid A architecture characterized by an asymmetric distribution of the acyl chains with respect to the DAG disaccharide backbone of the hexa-acylated species (4+2 arrangement). To sum up, the hexa-acylated family of lipid A originated from acyl-substitution at position 3 of the primary acyl chain located on the non-reducing DAG; both MS and MS/MS data suggested that the heterogeneity of this secondary fatty acids could be ascribed to mono and/or bis-hydroxylated 30:0, 31:0 and 32:0.

The third lipid A family was shifted to higher molecular mass by $\Delta m/z$ 512.4, the mass difference corresponding to a hepta-acylated structure carrying an additional hopanoid residue

(molecular formula $C_{34}H_{56}O_3$). The ion pattern in the MS/MS spectrum (Fig. 1c), following a fragmentation scheme similar to that previous observed, allowed us to draw the complete structure of the lipid A from *Bradyrhizobium sp.* BTAi1: the ion peak at *m/z* 2604.8corresponded to the hexa-acylated lipid A fragment lacking the residue of hopanoid (loss of 530 mass units*,* Fig. 1c) while the ion at *m/z*2111.3was the result of the loss of the whole *O*-acyloxyacyl group composed of the hopanoid residue linked to 32:0(2,31 2-OH). This finding indicated the hopanoid moiety as a tertiary substitution, located, as evinced from NMR analysis below, at the ω-1 position of the long chain fatty acid.

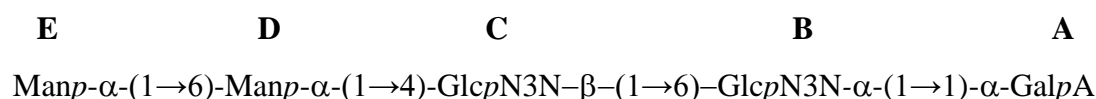## Supplementary Note 4

NMR spectroscopy of lipid A

For the NMR characterization, lipid A was dissolved in $CDCl_3/CD_3OD$ (^{1}H NMR spectrum in Supplementary Fig. 4a). A combination of homo- and heteronuclear 2D NMR experiment (DQF-COSY, TOCSY, TROESY, NOESY,^{1}H-^{13}C HSQC, ^{1}H-^{13}C HMBC, [1]J_{CH} HSQC) was executed in order to assign all the spin systems and to define the saccharidic sequence (Supplementary Table 2). The anomeric configuration of each monosaccharide unit was assigned on the basis of [1]$J_{C1,H1}$constants derived by *F2-coupled* HSQC (Supplementary Fig. 4b) and confirmed by the *intra*-residual NOE contacts. In the HSQC spectrum (Supplementary Fig.5) five cross peaks were located in the anomeric region, four signals, between 50 and 55 ppm, were attributable to nitrogen-bearing carbons, while in the region from 60 to 78 ppm resonated ring carbons as well as hydroxylated acyl chains and hopanoid moieties; other signals were clearly visible in the aliphatic and olephinic region. Coupling constants and chemical shift values were in agreement with the presence of two DAG residues, two residues of Man*p* and one of Gal*p*A, all present in $^4C_1$ chair conformation. In detail, the anomeric protons at 5.06 ppm (**B**) and 4.41 ppm (**C**) were respectively identified as α and β residues; their anomeric configuration was determined by the $^1J_{C1,H1}$ constants (Supplementary Fig. 4b and Supplementary Table 2) derived from *F2*-coupled HSQC measurements, and confirmed by the *intra*-residual NOE contacts observed in the ROESY spectrum (Supplementary Fig. 6a). Spin system **B** presented a $^1J_{C1,H1}$ value of 176 Hz and an *intra*-residual NOE contact of **B-**1 only with **B-**2, confirming the α-configuration. Spin system **C,** instead, presented a $^1J_{C1,H1}$ value of 162 Hz and NOE correlations of **C-**1 with **C-**2, **C-**3 and **C-**5, typical for a β-configuration. The carbon chemical shifts of **B**-2/**B**-3 (51.3/51.78 ppm) and **C**-2/**C**-3 (53.48/54.17 ppm) corresponded to *N*-linked carbons, in accordance with

the presence of DAG. The downfield shifts of the proton resonances of H-2 and H-3 of residues **B** and **C** were diagnostic for their *N*-acylation. The carbon resonance of **B**-6 (69.19 ppm) was evidently shifted downfield suggesting a glycosylation at this position. The anomeric proton of residue **C** presented a strong NOE correlation with **B**-6 suggesting that the two GlcN3N were β−(1→6)-linked, as confirmed by the corresponding long-range correlation.

Spin system **A** (5.22, 94.3 ppm) was assigned to an α-Gal*p*A residue. The $^3J_{\text{H3,H4}}$ and $^3J_{\text{H4,H5}}$ values (below 1 Hz) were in accordance with a *galacto*-configuration. The α-configuration was inferred by the heteronuclear $^1J_{\text{C1,H1}}$ value of 174 Hz, and confirmed by H-1/C-1 chemical shifts and by the *intra*-residual NOE contact of H-1 with H-2. The ring carbon resonances of **A** were not shifted downfield suggesting that this residue was terminal, in accordance with methylation analysis. The strong NOE contact between the anomeric protons of residues **A** and **B** and the long-range correlations between these two positions were diagnostic for their trehalose-like α,α−(1→1) linkage.

Residues **D** and **E** were α-Man*p* units. The *manno*-configuration was assigned by $^3J_{\text{H1-H2}}$ and $^3J_{\text{H2-H3}}$ values (below 3 Hz), whereas the anomeric configuration was established by the $^1J_{\text{C1,H1}}$ value and the *intra*-residual NOE contact of H-1 with H-2. The downfield shift of C-6 from residue **D** together with the strong NOE contact between **E**1 and **D**6'/**D**6" and the corresponding long range correlation (Supplementary Figs. 6a and 7, Supplementary Table 2) indicated that they were bound trough an α-(1→6)-linkage. Furthermore, the anomeric carbon of residue **D** presented a strong HMBC signal with H-4 from residue **C** (Supplementary Fig. 7) suggesting that the Man **D** was α-(1→4)-linked to the distal β-DAG unit.

In summary, all the NMR fully supported the existence of a pentasaccharide backbone formed by a skeleton of β−(1→6) linked DAG substituted by an α-GalA in trehalose-like α,α−(1→1) linkage on the vicinal DAG and by an α-(1→6) Man disaccharide α-(1→4)-linked to the distal β-DAG unit:

   E   **D**   **C**   **B**   **A**

Man*p*-α-(1→6)-Man*p*-α-(1→4)-Glc*p*N3N−β−(1→6)−Glc*p*N3N-α-(1→1)-α-Gal*p*A

A thorough analysis of the NMR spectra allowed us to further detail the spectroscopic characterization of the lipid A from *Bradyrhizobium* BTAi1. Several spin systems were

attributed to the acyl moieties. In the HSQC spectrum (Supplementary Fig. 5), the cross peaks at 3.83/68.1 ppm corresponded to H3/C3 of primary 14:0(3-OH) and 12:0(3-OH) moieties while the downfield signals at 5.29/71.32 ppm and 5.14/71.2 ppm were assigned to *O*-acylated H3/C3 of the same residues (Supplementary Figs. 6b and 7). The chemical shifts for α,β and γ atoms of 3-OH fatty acids are listed in Supplementary Table 2. In addition, two low field signals at 6.80/145.6 and 5.96/123.2 ppm and both correlated to an acyl carbon at 169 ppm were attributed to the double bond of a α,β unsaturated fatty acid (Δ2-FA, Supplementary Table 2, Supplementary Figs. 5-7). Interestingly, this unsaturated acyl moiety was clearly located at position 3 of the vicinal DAG, residue **B**, as evident from the long range correlation in the HMBC spectrum (Supplementary Fig. 7) between H3 **B** and C1 of Δ2-FA, as was further confirmed by the analysis of the MS spectra (see above).

The proton signal at 3.72 ppm correlated, in HSQC spectrum, to a carbon signal resonating at 67.3 ppm, was identified as the ω-1 methine of the long chain fatty acids, in turn connected to a methyl group at 1.15 ppm and to the ω-2 methylene protons at 1.4/1.38 ppm. Furthermore, NMR data also showed the correlation of a methyne group at 4.23/70.1 ppm with carbonyl and methylene groups (Supplementary table 2, Supplementary Fig. 6b), attributable to long chain fatty acids partially hydroxylated at position 2, in accordance to the chemical analysis (Supplementary Table 2). Analysis of the NMR spectra allowed to identify and locate the triterpenoid moiety constituting the hopanoid skeleton, in full accordance with the previously discussed GC-MS data. Particularly significant were the methyl signals resonating in the region between 0.6-1.0 ppm typical of the angular methyl constituents of the terpenoid moiety. The hopanoid resonances were attributed also on the basis of previously published data[1-3].Two further ω-1 methine groups (4.97/4.87 and 72.3/71.3 ppm respectively), were identified as *O*-acylated long chain fatty acid. The nature of their *O*-substitution was established as follow. The long range correlation present in the HMBC spectrum (Supplementary Table 2, Supplementary Fig. 7) between the ester carbon at 171.7 ppm, the ω−1 group of the LCFA at 4.87 ppm and the methyl acetyl group at 2.02 ppm was a proof of the *O*-acetylation of this lipid moiety. Furthermore, the long range correlation allowed to locate the hopanoid moiety on the second acylated LCFA. Actually, in the HMBC spectrum, the ester carbon at position 34 of the hopanoid moiety, Hop34, at 172.3 ppm, showed an *intra*-residual long range correlation with position 33 (Hop33) at 4.19 ppm and an *inter*-residual long range correlation with positions ω−1 of the LCFA at 4.97 pm, demonstrating the chemical linkage between the two moieties. Therefore, the hopanoid was attached, by an ester

linkage, at the ω−1 hydroxyl group of the long chain acyl moiety. In conclusion, the two VLCFA were esterified respectively by an acetyl group and a hopanoid residue.

Supplementary Note 5

Supramolecular arrangement of *Bradyrhizobium* cell envelope: role of lipid A and hopanoids in the stability of the outer membrane

In order to investigate by ESR the microstructure of membranes from*Bradyrhizobium*BTAi1 and BTAI1Δ*shc* mutant, the respective lipid A (Fig. 2 and Supplementary Fig. 9b) were included in the formulation of biomimetic liposomes prepared *in vitro*. Realistic models of the outer membrane of Gram-negative bacteria must incorporate lipid asymmetry, with all the LPS molecules in the outer leaflet of the lipid bilayer, the inner one being constituted by glycerophospholipids. For this reason typical methods for liposome preparation (e.g., sonication, extrusion, electroformation) have to be discharged. Different methods to prepare asymmetric liposomes have been presented in the literature. Partial asymmetry can be achieved by altering the distribution of specific phospholipids in pre-formed symmetric liposomes using external stimuli (e.g. pH gradients, osmotic pressure, or molecules that promote lipid redistribution).

However, the chemical constraints of these methods severely limit their applicability to our systems. In this work, we have adopted a protocol for asymmetric liposome preparation based on the assembly of two independently-prepared lipid monolayers[4]. It is the first time this method is used for liposomes including LPS and some modifications to the original protocol were required, as detailed in the method section (Fig. 7a and Supplementary Fig. 11). To determine the different physical properties of the two lipid leaflets, as derived from the different lipid composition, ESR spectra of spin-labelled lipids, purposely included in the liposome formulation, were registered[5-6].

The 5-PCSL spectra obtained for the lipid bilayers considered in this work at 30 °C are shown in Fig. 7b. As detailed in the experimental section, for each bilayer the molecular probe was inserted either in the outer leaflet or in the inner one.5-PCSL is a spin-labeled lipid bearing the nitroxide reporter group attached to the acyl chain in position 5, i.e. relatively close to the hydrophilic headgroup. Thus, it monitors the local structuring and dynamics of the lipid tails just underneath the polar interface between the membrane and the aqueous medium. The 5-PCSL ESR spectrum has been found to be highly sensitive to pseudo-phase transitions of lipid membranes from a disordered to an ordered state. In the disordered liquid crystalline state,

also named L_α, the carbon bonds in the lipid acyl chains presents both trans and gauche conformations rapidly interconverting, thus forming an hydrophobic core of the membrane closely resembling a liquid "oil". In the ordered states the acyl chains preferentially present all-trans conformations and tend to align in the same direction, thus forming a viscous and molecularly ordered hydrophobic core. Molecularly ordered membranes can be induced by a lowering of the temperature (solid or gel state, also named L_β) or by the presence of a guest molecule which "orders" the adjacent lipid chains (ordered liquid crystalline state, L_o). L_β and L_o membranes present the same short-range order constrains, only differing in long-range translation capabilities of the lipids along the bilayer, which is higher for the L_o membranes. From a macroscopic and functional viewpoint, both L_β and L_o membranes are more rigid and less permeable than L_α ones. Symmetric lipid bilayers formed by LPS usually present a transition from L_β to L_α with increasing the temperature above 20-25 °C. The presence of polycyclic compounds such as hopanoids, stabilizes an ordered L_o state even at higher temperature, thus improving the membrane strength and rigidity. In this respect, hopanoids serve the same function of sterols (e.g. cholesterol) in eukaryotes.

To the best of our knowledge, we have here reported the first investigation on the liquid crystalline state of asymmetric bilayers presenting one of the lipid leaflets (the outer one) predominantly composed by LPS. Here, we start with analyzing, as reference system, symmetric POPE/POPG bilayers. Inspection of Fig. 7b shows that 5-PCSL molecules present similar spectra when inserted in the outer or in the inner leaflet of such bilayers, thus confirming the symmetry of the membrane. The spectrum lineshape shows a marked anisotropy, as expected for spin-labels whose motions are significantly restricted by the neighboring acyl chains. The extent of this anisotropic behavior can be quantitatively estimated by measuring the outer hyperfine coupling constant, $2A_{max}$, defined as the distance, in Gauss, between the low-field maximum and the high-field minimum. In lipid bilayers, $2A_{max}$ is an index of the local ordering of the lipid chains and, consequently, of the membrane fluidity. The $2A_{max}$ values obtained by the analysis of all the spectra shown in Fig. 7b are collected in Supplementary Table 4, whose inspection confirms that the leaflet of symmetric POPE/POPG bilayers present the same behavior. Quantitatively, the observed $2A_{max}$ values indicated that the membrane was in the fluid L_α state[7].

As second lipid system, we considered asymmetric bilayers including HoLA in the outer leaflet formulation. The 5-PCSL spectra appear significantly affected by this insertion, showing a larger anisotropic lineshape for both bilayer leaflets, as also confirmed by the

increased $2A_{max}$ values reported in Supplementary Table 4. This evidence indicated that HoLA insertion in the outer leaflet caused a lower fluidity of the whole membrane, evocative of its mechanical strengthening. Unexpectedly, the inner leaflet was even more affected by HoLA presence than the outer leaflet, in which this lipid A had been positioned. This demonstrates that the long acyl chains of the lipid A from *Bradyrhizobium* BTAi1 passed through the membrane, so that the terminal hopanoid appendages were positioned in the inner leaflet (see the sketch in Fig. 7b). The result of this lipid arrangement is twofold: (i.) both leaflets were much more ordered and (ii.) the leaflets were tightly linked among them, the long acyl chains acting as a "tightrope" between the two membrane interfaces.

As third lipid system, we considered asymmetric lipid bilayers including lipid A from BTAI1Δ*shc* mutant in the outer leaflet formulation. In this case, the 5-PCSL spectra showed that the outer leaflet was less fluid than the inner one (see also Supplementary Table 4). Furthermore, the whole bilayer was less ordered that that in which the HoLA was present. This evidence indicated that the hopanoid moiety linked at a terminus of one acyl chain was essential to drive its insertion among the lipid chains of the opposite leaflet.

Finally, we considered a membrane whose outer leaflet contained the lipid A from BTAI1Δ*shc* mutant and hopanoid extracts. The 5-PCSL spectra and the $2A_{max}$ values showed that only the outer leaflet was affected by the hopanoid ordering effect, while the inner one remained almost unperturbed. It could be concluded that the long acyl chain was necessary to drive the hopanoid moiety to the inner leaflet, otherwise it tend to reside among the lipid A chains of the outer one. It is to be observed that lipid bilayers in which the outer and inner leaflet present a very different ordering, like the last we have considered, are usually unstable.

A further confirmation of our interpretation of 5-PCSL spectra comes from the spectra of 14-PCSL spectra inserted in the inner leaflet of the analyzed lipid systems, reported in Figure S12. As opposed to the clearly defined axially anisotropic spectra that are obtained for 5-PCSL, a narrower, three-line, quasi-isotropic spectrum is generally obtained for 14-PCSL, which bears the nitroxide reporter group attached to the acyl chain in position 14, i.e. close to the terminal methyl region of the chain. This flexibility gradient in segmental chain mobility, quantitatively confirmed by the $2A_{max}$ values reported in Supplementary Table 4, is a characteristic hallmark of the liquid-crystalline state of phospholipid bilayers. Perusal of the figure shows that the spectrum in bilayers including HoLA in the outer leaflet presents a second component, which is particularly evident in the low-field shoulder and high-field minimum highlighted by the arrows. This is clear evidence of a more ordered arrangement of the motionally restricted lipid tails, an effect of the long acyl chain insertion through both

lipid leaflets, the terminal hopanoid appendage acting as an anchor to the opposite bilayer surface (see the sketch in Fig. 7b).

Finally, the spectra of 5-PCSL inserted in the outer leaflet of either POPE/POPG symmetric bilayers or POPE/POPG/HoLA asymmetric bilayers were registered as a function of the temperature. The trends of the $2A_{max}$ values are shown in Supplementary Figure 14. In the case of POPE/POPG liposomes, a broad inflection is observed between 15 and 25 °C, corresponding to the increase in lipid chain mobility on the transition from the gel to the fluid phase. For POPE/POPG/HoLA asymmetric bilayers a much smoother decrease is observed, with no evident transition. Interestingly, HoLA increases the bilayer fluidity at low temperature, while causes its stiffening above ~15 °C.

In conclusion, all our results highlight that the molecular structure of HoLA is optimally suited to induce a high ordering of the bacterial asymmetric outer membrane, which results in its mechanical strengthening and stabilization.

Supplementary References

1. Costantino, V., Della Sala, G., Mangoni, A., Perinu, C. & Teta R. Blurring the BoundarybetweenBio- and Geohopanoids: Plakohopanoid, a C32 Biohopanoid Ester from Plakortiscf. lita, *Eur. J.Org. Chem.*, **2012**, 5171-5176 (2012).

2. Nytoft, H.P., Lutnæs, B.F. &Johansen, J.E. 28-Nor-spergulanes, a novelseries of rearrangedhopanes, *Organic Geochemistry***37**, 772–786 (2003).

3. Choma, A. &Komaniecka, I. Straight and branched (ω-1)-hydroxylatedvery long chainfattyacids are components of *Bradyrhizobium*lipid A. *Acta Biochim Pol.***58**, 51-8 (2011).

4. Pautot, S., Frisken, B. J.&Weitz, D. A. Engineering asymmetric vesicles. *Proc. Natl. Acad. Sci. USA.***100**, 10718-10721 (2003).

5. D'Errico, G. *et al.*Mesoscopic and microstructural characterization of liposomesformed by the lipooligosaccharide from *Salmonella minnesota* strain 595 (Re mutant). *Phys. Chem.Chem. Phys.*, **11**, 2314-2322 (2009).

6. D'Errico, G. et al. Characterization of liposomesformed by lipopolysaccharides from *Burkholderia cenocepacia*, *Burkholderia multivorans* and *Agrobacterium tumefaciens*: from the molecularstructure to the aggregate architecture. *Phys. Chem. Chem. Phys.***12**, 13574–13585 (2010).

7. D'Errico, G., D'Ursi, A. M. &Marsh, D. Interaction of a peptide derived from glycoprotein gp36 of Feline Immunodeficiency Virus and itslipoylatedanalogue with phospholipidmembranes).*Biochemistry*, **47**, 5317-5327 (2008).